Indoor Positioning Using Visible Light Communications

A Thesis

Presented to
the faculty of the School of Engineering and Applied Science
University of Virginia

in partial fulfillment
of the requirements for the degree

Master of Science

by

Zafer Vatansever

December

2015

APPROVAL SHEET

The thesis
is submitted in partial fulfillment of the requirements
for the degree of
Master of Science

AUTHOR

The thesis has been read and approved by the examining committee:

Maite Brandt-Pearce

Advisor

Stephen G. Wilson

Daniel S. Weller

Accepted for the School of Engineering and Applied Science:

Craig H. Benson, Dean, School of Engineering and Applied Science

December
2015

Acknowledgments

I would like to gratefully and sincerely thank my advisor, Professor Maite Brandt-Pearce for her guidance, understanding, patience, and most importantly, persistent encouragement and continuous support during my graduate studies at the University of Virginia.

It is a blessing to be surrounded by many colleagues and friends at the University of Virginia. I am grateful to all my friends in Charlottesville and for making my life at U.Va. enjoyable. I would like to personally thank Jie Lian for his contributions.

I would like to thank my country and my superiors for giving me this opportunity. At last but not at least, I would like to thank my wife, Serap for her love, my family for helping me become the person who I am today and my friend Sema Uyar for her support.

Zafer Vatansever

Charlottesville, Virginia

Abstract

The effort to provide accurate location based services has increased with the use of mobile devices. But there is no standard method for indoor localization and navigation services. Previous solutions in the literature are hard to implement in real life situations because they need modifications on the receiver. In this study, a visible light based indoor positioning–tracking method suitable for non–diffusing and diffusing lamp models is proposed. The received power from the light emitting diodes (LEDs) is used as sensor input, and then an extended Kalman filter is used for state estimation. We propose a method based on a map of power intensities in the room that is robust to low SNR, nonuniform power distributions, and intermittent measurements, and it does not require any modifications on the receiver side or on existing lighting structures. The results show that tracking errors around the resolution of the power map can be achieved using a non–diffusing lamp model.

Contents

List of Figures

List of Tables

List of Acronyms

AOA Angle of Arrival

cm Centimeter

dB Decibel

DC Direct Current

dm Decimeter

EKF Extended Kalman Filter

FET Field–Effect Transistor

FOV Field of View

GPS Global Positioning System

IMU Inertial Measurement Units

KF Kalman Filter

LBS Location Based Services

LED Light Emitting Diode

LOS Line of Sight

MAP Maximum A Posteriori

NN Nearest Neighbor

PD Photodetector

RSS Received Signal Strength

RSSI Received Signal Strength Indicator

SNR Signal to Noise Ratio

TOA Time of Arrival

RF–ID Radio Frequency Identification

RMSE Root Mean Square Error

UKF Unscented Kalman Filter

UWB Ultra Wide Band

VLC Visible Light Communications

VLP Visible Light Positioning

Wi–Fi Wireless Fidelity

σ Standard Deviation

Chapter 1

Introduction

Global positioning system (GPS) signals are subject to attenuation and losses in indoor environments since the signals cannot penetrate through buildings, walls or other obstacles. Indoor environment areas are smaller than outdoors, which makes the accuracy of GPS another concern; we need a higher accuracy for indoor areas. In this thesis we propose a highly accurate wireless user tracking and positioning system using visible light communications (VLC) based on an extended Kalman filter.

There is an increasing demand for location based services (LBS). The need for high accuracy indoor localization techniques is becoming essential to the increased connectivity capacity of mobile devices. Museums, warehouses, hospitals or malls are the potential areas where we need reliable positioning-navigation services. There are many solutions proposed to solve the indoor positioning-navigation.

In 1960, R. E. Kalman published his work which describes the solution to the discrete data linear filtering [1]. Since then the Kalman filter has probably become the most widely used method for autonomous, assisted navigation and sensor

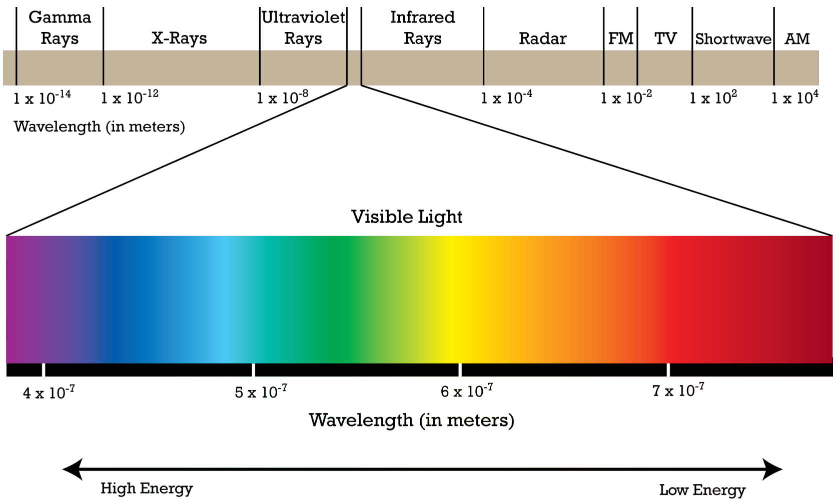

Figure 1.1: Electromagnetic spectrum [2].

fusion. The state estimation problem can be solved by using his mathematical framework in a recursive way. The Kalman filter minimizes the mean of the squared error.

Visible light is defined as the light that can be perceived by the human eye, which has a wavelength from 380 nm to 780 nm. The visible light is a small interval of the light spectrum. Figure 1.1 shows the visible light spectrum. It is in turn a small percent of the electromagnetic spectrum.

The emerging technology of visible light communication has led to developments in communications. It is a novel system that uses light emitting diodes (LEDs) for illumination and communication.

1.1 Research Motivation

In the last decade, research on indoor localization has become very popular. There are many different methods proposed to offer a solution for indoor localization. Especially, smart devices are in the center of the indoor positioning problem [3].

The proposed solutions are based on technologies such as wireless fidelity (Wi–Fi), ultra–wideband (UWB), radio-frequency identification (RF–ID), Bluetooth, inertial measurement units (IMUs) and visible light.

In the Wi–Fi approach, the received signal strength indicator (RSSI) is sent to a central processor. The processor tries to match the RSSI with the signal strength indicator map (fingerprints). This method may result in inaccurate estimations due to multipath errors in the measurements. The Wi–Fi approach is low cost, but it requires a database and it has low accuracy [4].

UWB indoor localization estimates the range or angle from multiple fixed points to a mobile target. Multilateration or multiangulation is used to process the measurements and find the position of the mobile user [5]. Time of arrival (TOA) and angle of arrival (AOA) measurements are not robust to noise. During sensor fusion, the noise in the measurements may lead to inaccurate estimates.

RF-ID based methods can be categorized into two: tag–oriented and reader–oriented. The tag–oriented approach tries to find the RF–ID tags. The reader–oriented approach finds the position of the reader. The advantages of RF-ID are simplicity, low-cost, portability, and high penetration capability [6]. The disadvantages are multipath effects, unstable RSSI and inaccuracy caused by one tag per location.

The Bluetooth approach compares the Bluetooth device signal strength to other Bluetooth devices. The measurements are sent to a central database to achieve indoor localization [7].

Inertial measurement units process the information from sensors like gyroscope, accelerometer. The drawback of this approach that is the initial position of the mobile user has to be known [4].

Visible light offers another solution for location based services (LBS). The effort to combine VLC and LBS has become popular since the emergence of visible light communications. Visible light communication based location services (VLC–LBS) can use all of the measurement types used above or can combine them.

The biggest advantage of using VLC instead of other approaches is electromagnetic interference. RF–ID, Wi–Fi and UWB create electromagnetic (EM) interference. EM interference is a limiting factor in areas like hospitals where sensitive devices are used. VLC is safer for human health. The competition for bandwidth between communication and positioning purposes causes a problem. Visible light can be used for both communication [8] and positioning [9]. Already installed illumination sources can be used without causing any electromagnetic interference, without side effects on communication services and installation costs.

In this thesis, a combination of Kalman filtering and VLC is proposed to solve the indoor positioning-navigation problem. The Kalman filter is used to fuse the measurements and estimate the state of the mobile user. Since the VLC power is a nonlinear function of the position, the extended Kalman filter (EKF) is chosen. We propose a solution to the indoor positioning and navigation problem using VLC and EKF.

1.2 Literature Review

In literature, there are three well known approaches to the indoor positioning problem: angulation - lateration, scene analysis and proximity [10]. The most commonly used measurement types in these approaches are received signal strength indicator (RSSI), time of arrival (TOA) and angle of arrival (AOA) measurements [9].

In [11] the RSSI is used to calculate the distance between reference and user. Later a circular lateration is used to get the position of the mobile user. In [12] angulation is used. Sensors that can sense signal strength, azimuth and elevation are combined to compensate the angulation errors. In [13], multiple and uncoordinated light sources are used for angulation. User involvement is investigated when there are ambiguities caused by uncoordinated light sources.

Scene analysis approach is used in [14], where the known reference points are matched with RSSI. The positioning problem is solved by matching RSSI to the closest reference point. The drawback of this approach is pre–calibration. If the power distribution in the room changes, it will take time to calculate and calibrate the new distribution.

The proximity approach requires a dense grid of illumination and probably is the most expensive approach. This approach is used in [15].

In [16], unique frequency addresses are assigned to each of the LEDs on the lamps, and the phase difference measurements, a variation of time difference of arrival (TDOA) are used. However this study requires two sensors with known distances between them.

In [17], a Kalman filter is used for state estimation using VLC. The performance of extended and unscented Kalman filters is compared for handover between luminaries. In this study, it is assumed that the geometry between the transmitter and the receiver is known, so that they can linearize the channel model.

Angle of arrival (AOA) relies on the precise design of the lenses. According to [9], this method is the most promising one. Tilted multiple photodetectors and a single transmitter are used in [18]. The study is based on gain difference, a function of RSSI and AOA. A real time study, which combines AOA measurements and image processing is [19]. In [20], AOA and RSSI are combined again.

Although AOA measurements are thought to be the future standard in [9], we can see that RSSI measurements are involved or combined in almost every study in the literature.

1.3 Thesis Outline

In this thesis, we first introduce the VLC channel model, and then we introduce a diffusing lamp model with random angles to imitate the behavior of a chandelier. Then we discuss the existing indoor visible light positioning approaches and common measurement types. We propose a new approach with the extended Kalman filter for indoor positioning. Finally, we compare the performance of EKF and the performance of trilateration with different lamp models.

The rest of the thesis is organized as follows: in Chapter 2, we analyze the channel and transmitter characteristics and evaluate the performance using simulations. Chapter 3 is about the indoor localization methods using VLC. A detailed review of different approaches is presented. Chapter 4 introduces the Kalman filter approach and we give information about the noise sources in the system, and how we obtain the floor power distribution when we use a diffusing lamp. In Chapter 4, we also show the simulation performance results of our approach and compare the results with the trilateration approach. Chapter 5 summarizes the entire thesis and discusses future work and applications.

Chapter 2

Visible Light Communication Channel and Transmitter Models

Visible light communication is the backbone of the indoor positioning algorithm. In this chapter, the relationship between transmitter and receiver, and the channel gain is explained. One goal of this study is to show the effect of the transmitter on positioning performance. The channel model and transmitter models give us the floor power distributions and the impulse response.

2.1 Indoor Visible Light Communication Channel Model

This section discusses indoor VLC channel model and the derivation of the channel model with a 25-LED lamp model. Understanding the VLC channel will lead us to design better indoor positioning systems. In this study, white LEDs are transmitters (sources). The photodetector on a mobile platform is the receiver.

Since the visible light is incoherent, intensity modulation and direct detection are employed in VLC systems. The signal on receiver side can be depicted as shown in Figure 2.1.

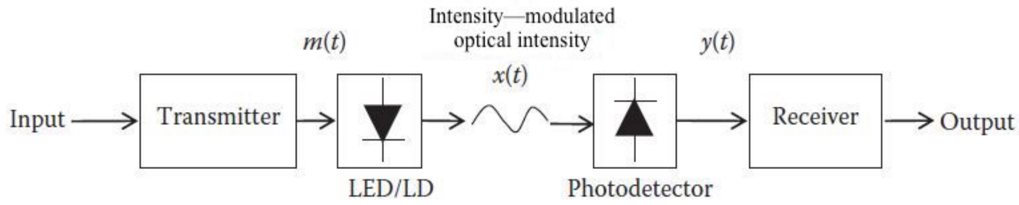

Figure 2.1: Optical intensity modulation, direct detection communications channel [2].

Figure 2.1 represents an optical intensity modulation and direct detection channel. The input signal is modulated with signal $m(t)$. Signal $x(t)$ has varying optical intensities as a result of modulation. The carrier signal $x(t)$ is detected by a photodetector. The optical output signal is $y(t)$.

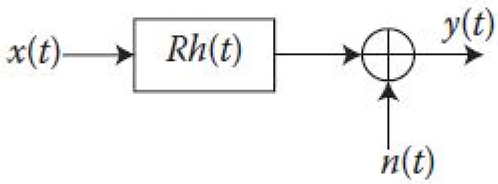

Figure 2.2: Simplified model of communications channel.

Figure 2.2 shows a simplified communication channel model. $y(t)$ is the received signal. $x(t)$ is the transmitted optical intensity, R is the detector responsivity and $n(t)$ is the additive noise. $h(t)$ is the indoor channel impulse response. $h(t)$ can be modeled from ray tracing. Mathematically, the system can be written as

$$y(t) = x(t) * Rh(t) + n(t), \tag{2.1}$$

where,

$$h(t) = \sum_{n=1}^{N} a_n \delta(t - t_n), \tag{2.2}$$

a_n and t_n are the path gains and transmission delay times, respectively of the various rays. They depend on the path of light rays between transmission and receiver. N is the number of multipath components.

There are two kinds of light rays in VLC channel. The line-of-sight (LOS) ray is the main component, and diffused ray that are weaker. In this study we only consider the LOS; otherwise no tracking can be achieved. The multipath effect in indoor VLC is a result of these rays. The indoor VLC channel transfer function is given by [2]

$$\mathscr{F}[h(t)] = H(f) = H_{LOS}(f) + H_{diff}(f). \tag{2.3}$$

H_{LOS} is the line of sight component. H_{diff} is the diffused component. The contribution of diffused rays of light is less than line-of-sight component.

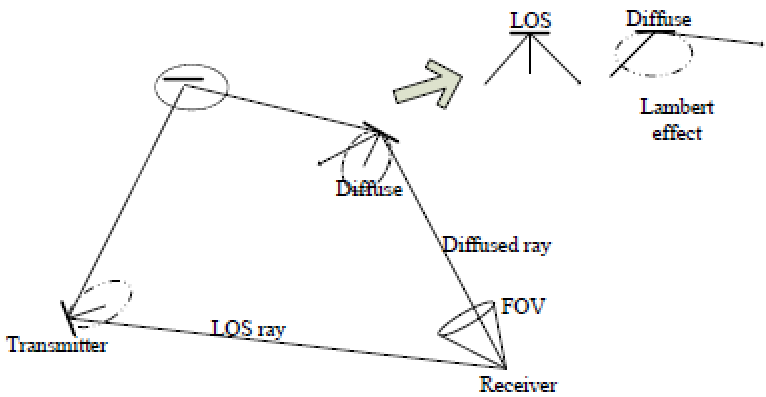

Figure 2.3: Line-of-sight and diffusion components of rays of light [21].

We assume that H_{LOS} is independent of the frequency flat channel, it depends only on the distance between transmitter and receiver.

The rays of light travel through the air, according to the Lambertian law. Lambert's law states that the radiant intensity depends on angle ϕ between the direction of the incident light and the surface normal. Lambertian radiant intensity is given by [22]

$$m = \frac{ln2}{ln(cos\Phi_{1/2})}, \tag{2.4}$$

$$R_0(\phi) = \begin{cases} \frac{m+1}{2\pi} cos(\phi), & \text{for } \phi \in [-\pi/2, \pi/2], \\ 0, & \text{for } |\phi| \geqslant \pi/2, \end{cases} \tag{2.5}$$

m is the Lambertian mode of the light source, $R_0(\phi)$ is the Lambertian radiant intensity, ϕ is the radiation angle relative the transmitter boresight. $\Phi_{1/2}$ is the semi angle of the LED. When $\phi = 0$, the radiated power is at a maximum. A_{eff} is the detector effective area:

$$A_{eff}(\psi) = \begin{cases} A_r cos\psi, & \text{if } -\pi/2 \geqslant \psi \geqslant \pi/2, \\ 0, & \text{if } |\psi| > \pi/2, \end{cases} \tag{2.6}$$

The detector effective area is a function of the incident angle, ψ. The detector has a field of view (FOV) angle, Ψ_c. Beyond Ψ_c, the detector does not detect light.

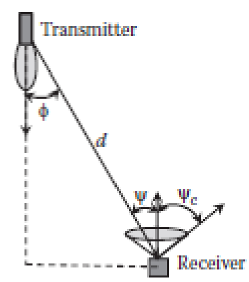

Figure 2.4: Geometry of LOS propagation model [2]

The line-of-sight link gain is given by

$$H_{LOS} = \begin{cases} A_r \frac{m+1}{2\pi d^2} cos^m(\phi) cos(\psi), & \text{if } -\Psi_c \geqslant \psi \geqslant \Psi_c, \\ \\ 0, & \text{elsewhere}, \end{cases} \tag{2.7}$$

The received power on the receiver (P_r) is a function of the line–of–sight link, (H_{LOS}) and the transmitted power from the luminary (P_t) and is given by

$$P_r = H_{LOS} \times P_t. \tag{2.8}$$

For completeness, the impulse response of the LOS component and the reflected components are given by

$$h_{LOS}(t) = A_r \frac{m+1}{2\pi d^2} cos^m(\phi) cos(\psi) \delta\left(t - \frac{d}{c}\right), \tag{2.9}$$

$$h_{diff}^{(k)}(t) = A_r L_0 L_1 L_2 \ldots L_k \gamma \delta\left(t - \frac{d_0 + d_1 + \ldots d_k}{c}\right), \tag{2.10}$$

$$L_0 = \frac{(m+1) cos^m(\phi_0) cos(\psi_0)}{2\pi d_0^2}, \tag{2.11}$$

$$L_1 = \frac{cos^m(\phi_1) cos(\psi_1)}{\pi d_1^2}, \tag{2.12}$$

$$\vdots \tag{2.13}$$

$$L_k = \frac{cos^m(\phi_k) cos(\psi_k)}{\pi d_k^2}, \tag{2.14}$$

$L_0, L_1, \ldots, L_k$ are the link attenuations, γ is the reflection coefficient. d_0 is the distance between the transmitter and receiver for LOS. d_k is the distance of the kth bounce link. ϕ and ψ are the irradiation and incidence angles, respectively, and c is the speed of light [23]. In this study, we only consider the LOS.

2.2 Transmitter Models

The transmitter model plays an important role in VLC. The transmitter is the LED light bulb in this study. The received power depends on the transmitter as much as the channel. One previous transmitter model, the deterministic 25-LED lamp proposed in [21] and a modification of the deterministic 25-LED lamp are used. The purpose of the modification on the 25-LED lamp is to imitate the behavior of a diffusing lamp. Diffusing lamps like chandeliers are used in large areas, especially museums and conference halls.

In a conventional LED bulb, the LEDs are facing downwards. As a result, a small area, where the bulb points, is illuminated. A large array of LEDs may be needed to cover larger areas.

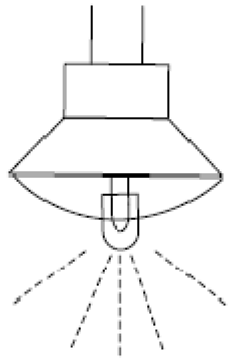

Figure 2.5: Illumination pattern of a conventional LED lamp [21].

2.2.1 The 25-LED Bulb Model

The 25-LED lamp model has three layers of LEDs. This lamp model is deterministic. The layers consist of 1, 8, and 16 LEDs, respectively. Each LED has individual inclination angles. The purpose of this layout is to illuminate more area [21]. The DC channel gain for a LOS link between ith LED and the kth receiver can be rewritten as

$$H_{ik} = A_r \frac{cos\langle \vec{r}_{ik}, \vec{n}_k \rangle}{2\pi d_{ik}^2}(m+1)cos^m\langle \vec{r}_{ik}, \vec{l}_i \rangle, \tag{2.15}$$

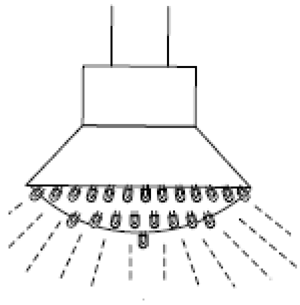

Figure 2.6: Illumination pattern of a 25-LED lamp [21].

In (2.15), d_{ik} is the distance between the ith LED and kth receiver. $\vec{r}_{ik}$ is the unit vector from tth LED to kth receiver. $\vec{n}_k$ is the kth receiver's normal unit vector. $\vec{l}_i$ is the radiation unit direction vector for ith LED. $\langle \vec{r}_{ik}, \vec{n}_k \rangle$ is the angle between the direction of ith LED and receiver k.

2.2.2 Diffusing Lamp Model

The diffusing model is based on the 25-LED lamp model. Each LED has a random inclination angle. These angles imitate the diffuser. This model assumes the random refraction of light as it travels through a diffuser like the crystal prisms of a chandelier. We try to model the propagation of light after the diffuser. As a result of random angles, the power distribution on the floor is significantly less uniform than without a diffuser. Figure 2.7 shows the random irradiance angles of rays of light. With this modification, the channel gain formula (2.15) becomes

$$H_{ik} = A_r \frac{cos\langle \vec{r}_{ik}, \vec{n}_k \rangle}{2\pi d_{ik}^2}(m+1)cos^m(\langle \vec{r}_{ik}, \vec{l}_i \rangle + \theta), \tag{2.16}$$

The random inclination angle is denoted as θ. θ is a Gaussian random variable with zero mean and variance σ.

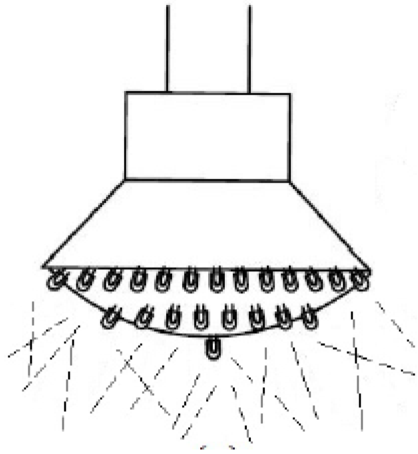

Figure 2.7: Illumination pattern of a diffusing lamp.

2.3 Indoor Channel and Power Distribution Maps

The performance of the deterministic 25-LED lamp and the random 25-LED lamp model is shown for different LED semiangles. The standard illumination level at a height of 0.8 m is 220 lux [24].

For positioning purposes, we would like to illuminate as much area as possible. If the illumination is concentrated under the light bulbs, this set up will decrease the positioning performance, as the signal–to–noise ratio will be low in the non-illuminated areas and corners. Figures 2.8–2-10 show the relationship between the LED semiangle and illuminated area coverage. The simulations parameters for the room conditions is given in Table 4.1, we see that the larger semiangle yields better illumination levels on the room floor. The highest illumination level is achieved when the LED semiangle is 10°. The light is concentrated under the light bulbs in this scenario. For communication privacy purposes, this model is acceptable, but as you move away from the source, the positioning and communication performance decreases. When the LED semiangle is 30°, the illumination coverage will be increased, but it will still not cover the room. Therefore we choose a 60° semiangle.

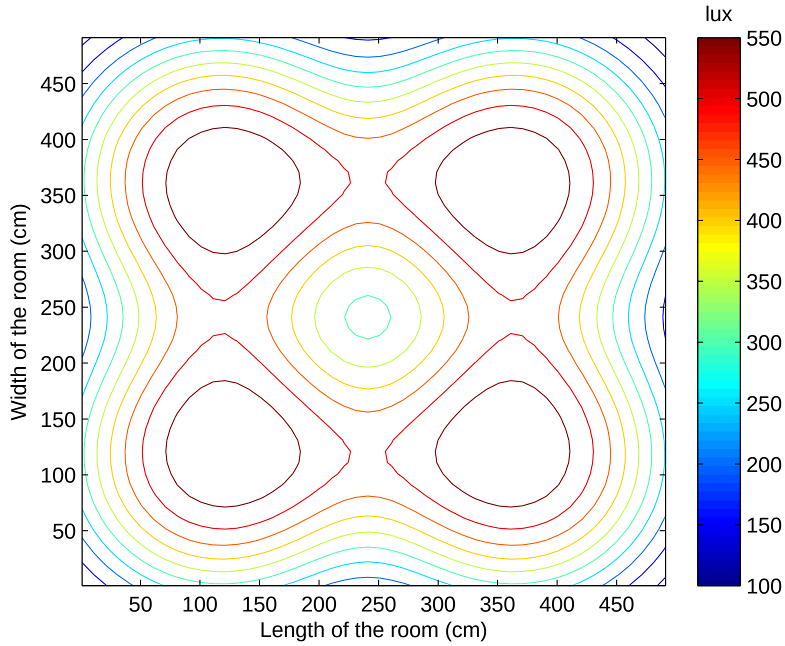

Figure 2.8: Power distribution on the floor for 25-LED. LED semiangle 10°.

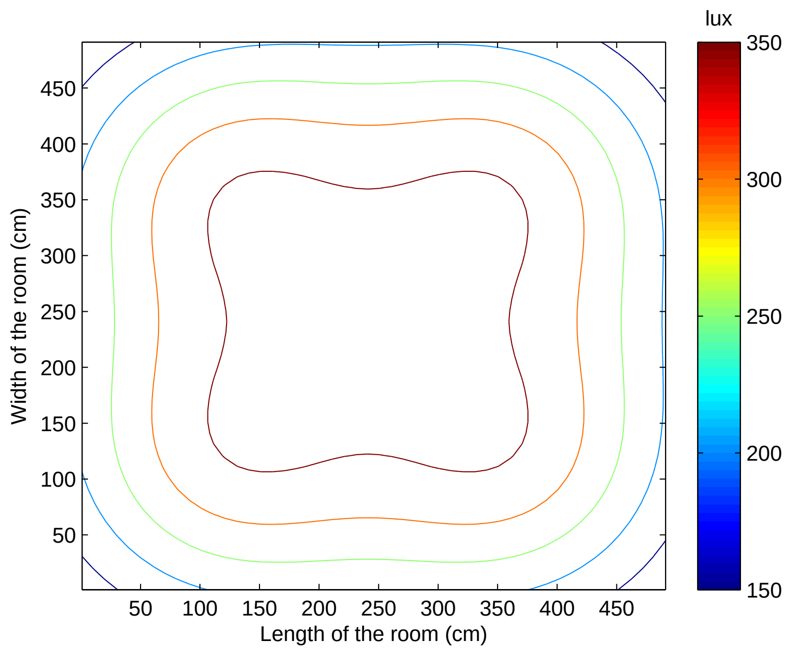

Figure 2.9: Power distribution on the floor for the deterministic 25-LED. LED semiangle 30°.

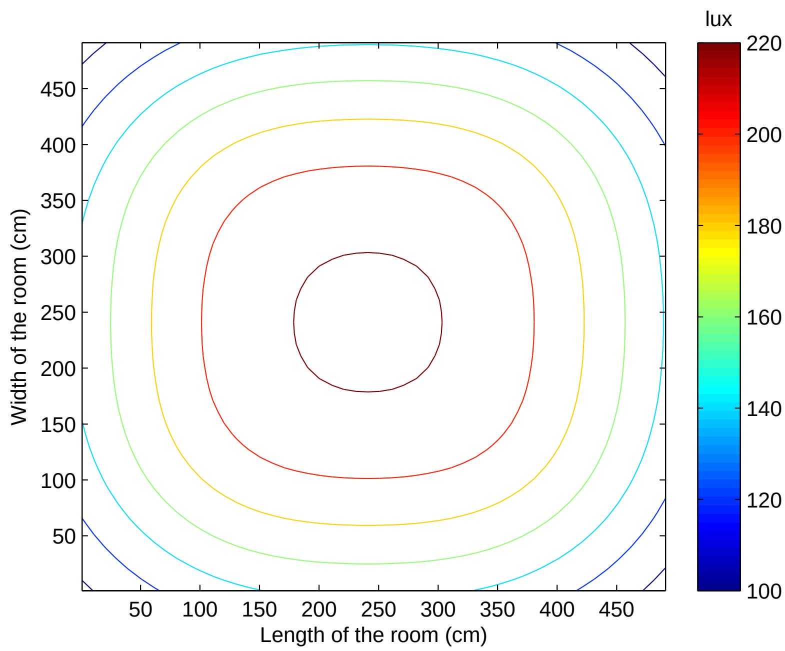

Figure 2.10: Power distribution on the floor for the deterministic 25-LED. LED semi-angle 60°.

Figures 2.11–2.13 show the illumination distribution when the diffusing lamp model, for example, a chandelier, using a standard deviation (σ) of 30°. The random inclination angles of LEDs result in a unique distribution. If the LED semiangles are 10° and 30° respectively, the same illumination performance as the 25-LED lamp is observed. Although the illumination is high in the middle, the corners are not well illuminated. For the 60° semiangle, the difference of illumination contours is not as high as other semiangle values.

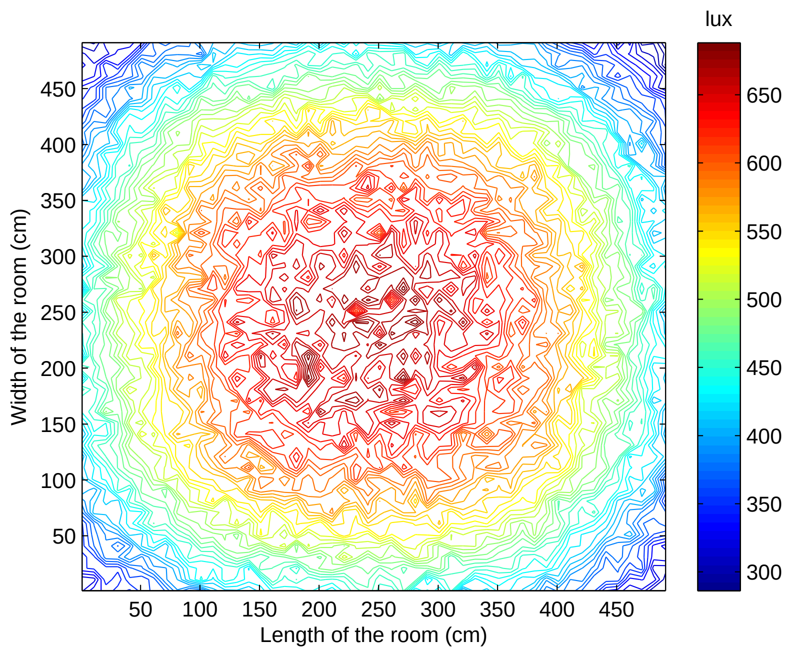

Figure 2.11: Power distribution on the floor for the diffusing lamp model. LED semiangle 10°.

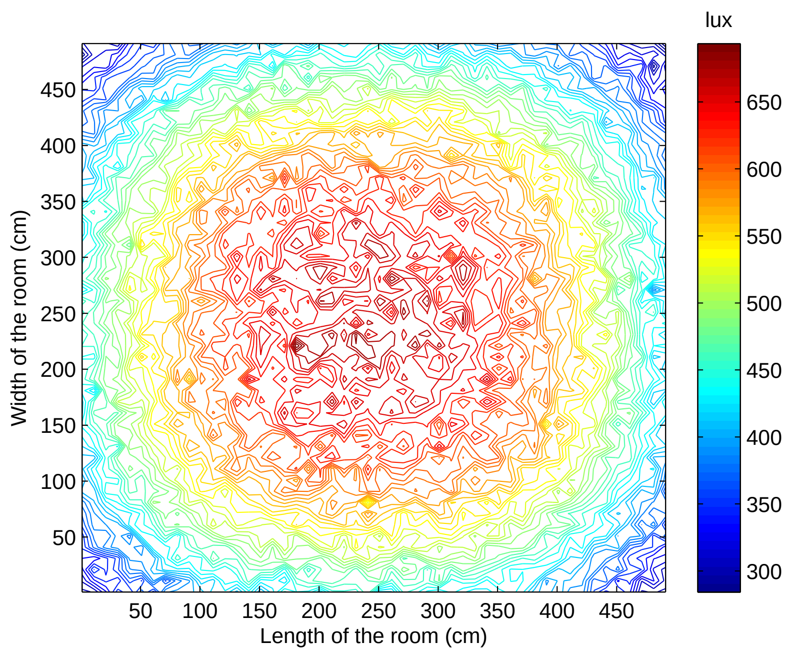

Figure 2.12: Power distribution on the floor for the diffusing lamp model. LED semiangle 30°.

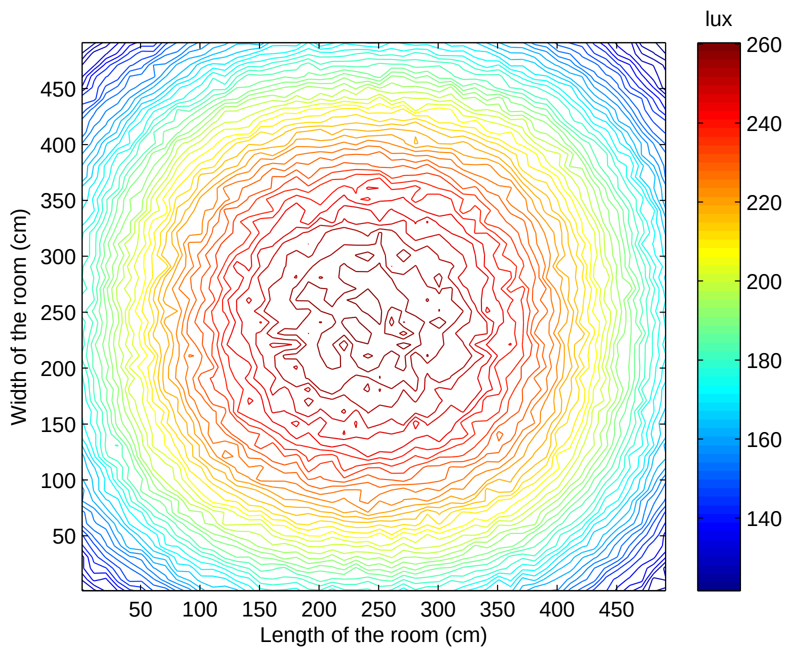

Figure 2.13: Power distribution on the floor for the diffusing lamp model. LED semiangle 60°.

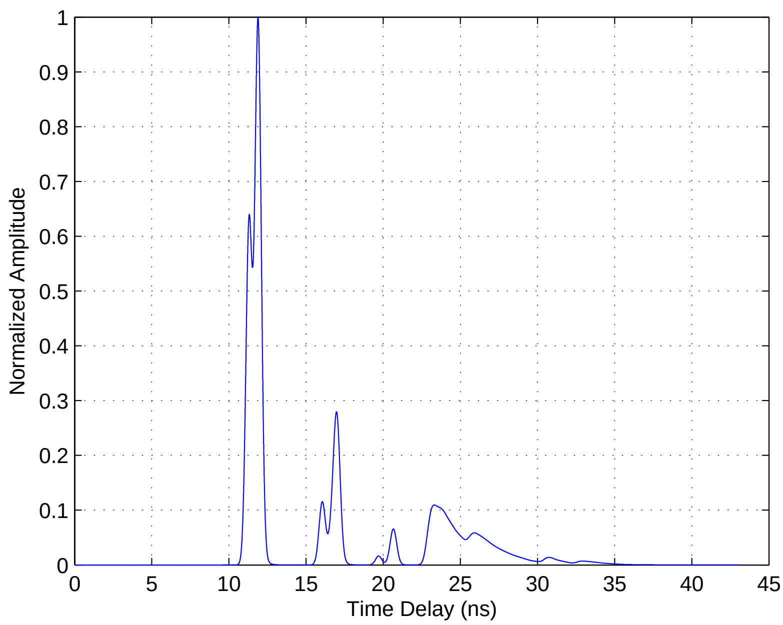

Figure 2.14: Normalized impulse response of the deterministic 25-LED lamp semiangle 60° at the room center.

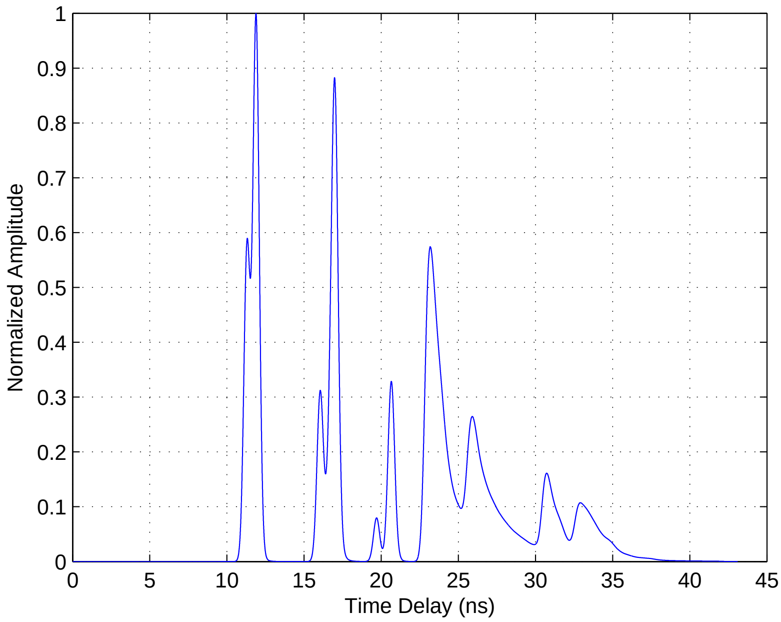

Figure 2.15: Normalized impulse response of the diffusing lamp model semiangle 60° at the room center.

For the 25-LED lamp the impulse response with a semiangle 60° for a receiver in the center of the room is shown in Figure 2.14. The size of the room is $5 \times 5 \times 3\ m^3$. The impulse response of a diffusing lamp with the same LED semiangle is shown in Figure 2.15. We observe that the dispersion is more than the deterministic 25-LED lamp model. This results in a stronger multipath effect than the deterministic 25-LED lamp case.

Chapter 3

Indoor Localization Methods Using Visible Light Communications

Positioning or localization is the process of finding the most accurate location of an object. The increasing computational capacity of mobile devices such as cell phones and tablets has created an opportunity for indoor positioning methods. If we enter a building and look up, we will see the lighting fixtures. The advances in VLC make it one of the best candidates for solving location based problems. The installation cost is lower than Wi–Fi or RF–ID methods.

The target market for visible light positioning (VLP) consists of areas where a large number of people and items are available. The aim is to find the accurate location of the user and try to navigate the user to the target, just like a Global Positioning System (GPS). Large warehouses, museums, shopping malls, hospitals, hotels and conference halls are areas where people need location knowledge.

According to [25], the market for location based services (LBS) has tripled since 2012. In this chapter, the advantages of VLP, positioning approaches for VLP and challenges will be discussed.

3.1 Advantages of Visible Light Positioning (VLP)

GPS is the best solution for outdoor positioning for now, but the radio waves of GPS are subject to multipath effects because radio waves reflect from humans or other kind of obstacles. The accuracy of GPS is also another concern, for an indoor area an inaccuracy of a couple of meters is big. But indoor VLP signals do not suffer any power loss, unless there is an obstacle blocking the LOS.

Bandwidth is also another concern for communication purposes. Visible light users do not compete for bandwidth like in Wi–Fi. The light waves cannot penetrate through solid materials generally, which makes VLC a reliable and secure network medium. So there will be no interference with neighboring rooms. Since there is no interference and there are less multipath effects, VLP systems give more accurate results than other methods.

3.2 Measurement Types in Visible Light Positioning

In this section, we will briefly talk about measurement types used in VLP for a broader understanding of the topic. The advantages and disadvantages of the type of measurement will also be discussed.

The most used measurement type is the received signal strength (RSS). The received power on the receiver is measured. RSS knowledge may help us to calculate the distance between the transmitter and the receiver. RSS may also be used to map the target area, for example a room floor. This method is also known as fingerprinting [26]. The RSS may be used in a nearest neighbor (NN) algorithm to locate the object. Common assumptions for this kind of measurement are that the transmitted optical power is known, and that the transmitter and receiver relationships are known [9].

Time of arrival (TOA) is the measurement type used in GPS but it is hard to measure for a VLP system. The synchronization must be perfect between transmitters. Time difference of arrival (TDOA) is a modified method that eliminates the requirement for synchronization [27]. However, the indoor environments are small and the speed of light is huge. TDOA requires very precise equipment for accurate positioning. Low signal-to-noise ratio may lead to big errors.

Angle of arrival (AOA) is meaningful if only LOS is unblocked and clear. The lenses used in mobile devices are precise and accurate, which reduces any uncertainty.

3.3 Positioning Algorithms

3.3.1 Lateration and Angulation

Triangulation method takes advantage of geometrical equations and least square method to solve the positioning problem. Almost all types of measurements are used. Angulation is the method when AOA measurements are used. In lateration, RSS, TOA and TDOA are used [28]. At least three intersecting spheres are needed

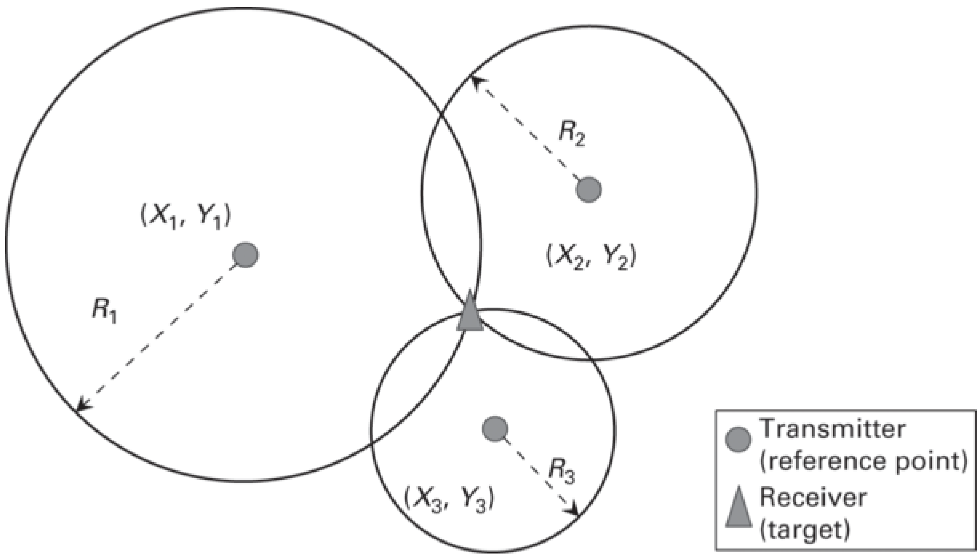

Figure 3.1: Circular lateration [10].

for positioning.

RSS based lateration methods assume that the geometric relationship between the transmitter and receiver is known. The reference points are LED luminaries with known positions. The channel model is used to calculate the distance between the source and the user. The distance calculation for RSS is given in the following equation [11]

$$P_r = P_t A_r \frac{m+1}{2\pi d^2} cos^m(\phi) cos(\psi), \tag{3.1}$$

$$d_{xyz} = \sqrt{P_t A_r \frac{m+1}{2\pi P_r} cos^m(\phi) cos(\psi)}, \tag{3.2}$$

$$d_{xy} = \sqrt{d_{xyz}^2 - d_z^2}, \tag{3.3}$$

$$cos(\phi) = cos(\psi). \tag{3.4}$$

P_r is the RSS on the receiver, P_t is the transmitted power from the source. $cos(\phi)$ is the angle of irradiance and $cos(\psi)$ is the incidence angle. d_{xyz} is the three dimensional distance between source and receiver. d_{xy} is the two dimensional distance.

Given the distance from light sources, the trilateration problem is solved as a least squares problem. The equation of a circle is the starting point for trilateration. Figure 3.1 depicts how circles are used for lateration. The solution of lateration is given as

$$(X_i - x)^2 + (Y_i - y)^2 = R_i^2, \tag{3.5}$$

$$R_i^2 - R_1^2 = (x - X_i)^2 + (y - Y_i)^2 - (x - X_1)^2 - (y - Y_1)^2, \tag{3.6}$$

$$= X_i^2 + Y_i^2 - X_1^2 - Y_1^2 - 2x(X_i - X_1) - 2y(Y_i - Y_1). \tag{3.7}$$

(X_i, Y_i) is the position of the ith transmitter in a 2D plane. (x, y) are the position of the receiver. If R_i is the distance between transmitter and receiver, a circle with radius of R_i is a possible solution where (x, y) can be. $i = 1, 2, \ldots, n$ and n is the number of transmitters. Now the least squares solution of the above is as follows:

$$AX = B, \tag{3.8}$$

$$X = [x\ y]^T, \tag{3.9}$$

$$A = \begin{bmatrix} X_2 - X_1 & Y_2 - Y_1 \\ \vdots & \vdots \\ X_n - X_1 & Y_n - Y_1 \end{bmatrix}, \tag{3.10}$$

$$B = \frac{1}{2} \begin{bmatrix} (R_1^2 - R_2^2) + (X_2^2 + X_2^2) - (X_1^2 + Y_1^2) \\ \vdots \\ (R_1^2 - R_n^2) + (X_n^2 + X_n^2) - (X_1^2 + Y_1^2) \end{bmatrix}, \tag{3.11}$$

$$X = (A^T A)^{-1} A^T B. \tag{3.12}$$

Hyperbolic lateration is an extension of lateration. TDOA measurements are used in this approach. At least two light sources are needed. We may begin the

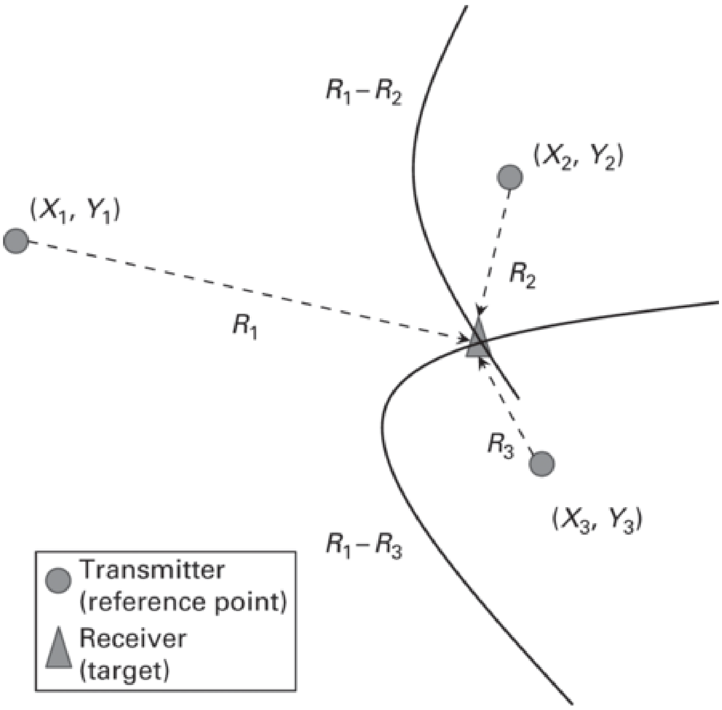

Figure 3.2: Hyperbolic lateration [10].

solution from a hyperbola equation

$$d_{ij} = R_i - R_j \tag{3.13}$$

$$= \sqrt{(X_i - x)^2 + (Y_i - y)^2} - \sqrt{(X_j - x)^2 + (Y_j - y)^2}, \tag{3.14}$$

$$(R1 + D_{i1})^2 = R_i^2, \tag{3.15}$$

$$X_i^2 + Y_i^2 - X_1^2 - Y_1^2 - 2x(X_i - X_1) - 2y(Y_i - Y_1) - D_{i1} - 2D_{i1}R_1 = 0, \tag{3.16}$$

$$AX = B, \tag{3.17}$$

$$X = [x\, y\, R1]^T, \tag{3.18}$$

$$A = \begin{bmatrix} X_2 - X_1 & Y_2 - Y_1 & D_{21} \\ \vdots & \vdots & \\ X_n - X_1 & Y_n - Y1 & D_{n1} \end{bmatrix}, \tag{3.19}$$

$$B = \frac{1}{2} \begin{bmatrix} (X_2^2 + Y_2^2) - (X_1^2 + Y_1^2) - D_{21}^2 \\ \vdots \\ (X_n^2 + Y_n^2) - (X_1^2 + Y_1^2) - D_{n1}^2) \end{bmatrix}, \tag{3.20}$$

$$X = (A^T A)^{-1} A^T B. \tag{3.21}$$

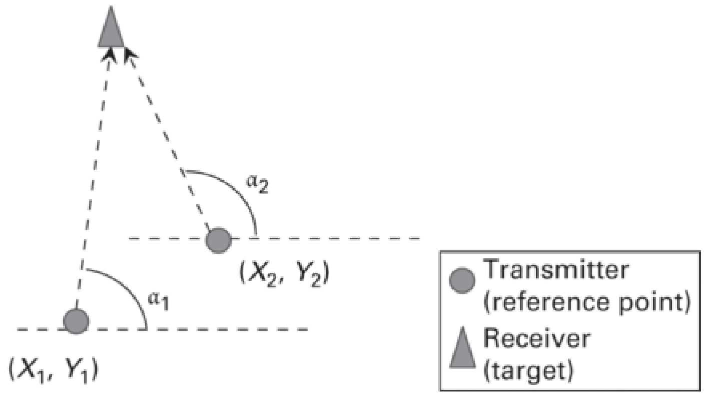

Figure 3.3: Angulation[10].

In the angulation method, intersection of lines is used to find the receiver's position. High quality imaging sensors make it easier to detect the angular information compared to methods that use antennas [9]. The least squares approach is used to solve the angulation equations.

$$\tan \alpha_i = \frac{y - Y_i}{x - X_i}, \tag{3.22}$$

$$(x - X_i) \sin \alpha_i = (y - Y_i) \cos \alpha_i, \tag{3.23}$$

$$AX = B, \tag{3.24}$$

$$X = [x\, y]^T, \tag{3.25}$$

$$A = \begin{bmatrix} -\sin \alpha_1 & \cos \alpha_1 \\ \vdots & \\ -\sin \alpha_n & \cos \alpha_n \end{bmatrix}, \tag{3.26}$$

$$B = \begin{bmatrix} Y_1 \cos \alpha_1 - X_1 \sin \alpha_1 \\ \vdots \\ Y_n \cos \alpha_n - X_n \sin \alpha_n \end{bmatrix}, \tag{3.27}$$

$$X = (A^T A)^{-1} A^T B. \tag{3.28}$$

3.3.2 Scene Analysis

In this approach, the previously defined points are used as reference (anchor) points. The RSS is not the only measurement type used, but generally RSS is easier to match with anchor points. The biggest advantage is that the computation time required for the matching process is less than angulation and lateration. It is a simple method, which does not require much computation. However, scene analysis requires the entire RSS information and information of anchor points. If there is a change in the scene, then the whole scene needs to be analyzed and anchors need to be recalculated. A preparation phase is needed to use the system in an effective and accurate way.

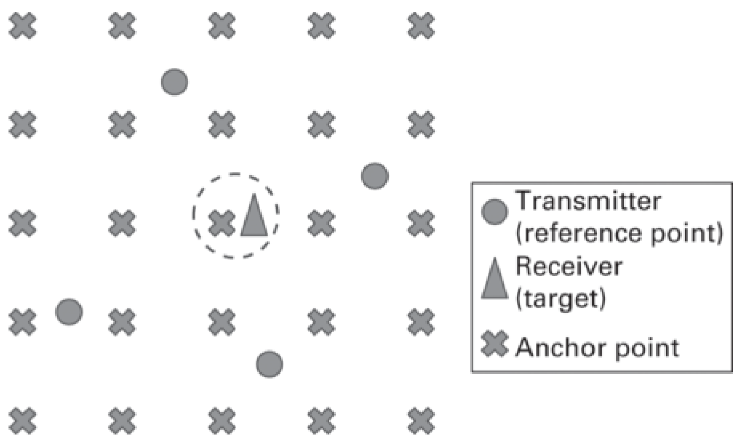

Figure 3.4: Scene analysis [10].

Figure 3.4 shows how the scene analysis approach works. The fingerprints are collected in the calibration phase. Then some of these fingerprints are used as reference points. The measurement is matched with the closest reference point.

3.3.3 Proximity

Proximity or closeness is an approach that requires light sources with known ID and position. The received signal is matched with the closest source. The accuracy of this approach depends on the number of light sources, on a dense grid of sources. If the density of the grid is high, then interference of signals may occur, which is prevented by either using a small LED semiangle or averaging of the received signals.

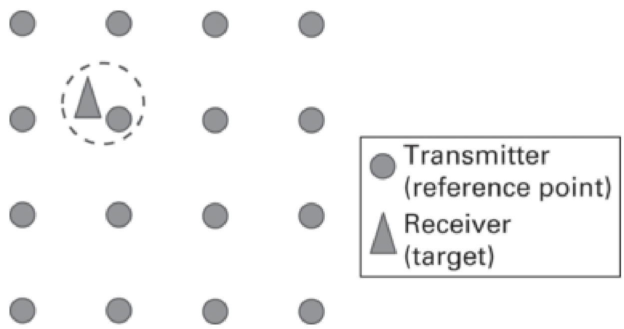

Figure 3.5: Proximity [10].

Figure 3.5 depicts the proximity approach; the received information from the transmitter is matched with the closest light source.

Table 3.1 is a comparison of the previous work published in the VLC positioning context. The measurement types used, the advantages and disadvantages are listed. Table 3.1 shows that the most of the methods use lateration–angulation approaches.

Table 3.1: Comparison of previously published work

Algorithm	Measurement	Reference	Accuracy	Advantages	Disadvantages
Trilateration	RSS	[10]	6 cm	Easy to implement	Susceptible to noise, Geometry between source and receiver must be known
Triangulation	RSS- AOA	[11]	14 cm	Two step approach to increase accuracy	Complicated system architechture, Geometry
Triangulation	RSS	[12]	0.4 m	Can work with a single LED	Inaccuary
Proximity	RSS	[13]	4.38 cm	Easy to implement	Requires a dense grid of illumination
Hybrid	AOA	[14]	-	Hybrid system	Complexity
Trilateration	RSS	[15]	0.5 mm	Can be used for 3-D positioning	Susceptible to noise, First order Lambertian emission assumed
Scene Analysis	RSS	[16]	4 cm	Easy to implement	Calibration needed
Trilateration	TDOA	[17]	1 cm	High accuracy	Susceptible to noise
State Estimation	RSS	[18]	5-10 cm	Easy to implement	Initial conditions must be well defined
Hybrid	AOA - RSS	[19]	6 cm	3D positioning	Computationally expensive
Triangulation	AOA	[20]	10 cm	-	Complexity
Triangulation	TDOA	[29]	1.8 mm	Early TDOA application	Complexity
Triangulation	AOA	[30]	4.6 cm	Early AOA application	Complexity

Chapter 4

Positioning Method

In this chapter, the proposed positioning method is explained. A thorough explanation of building blocks for our method is discussed. First, the Kalman filter, which is the heart of the positioning method, is described. Then, the dynamic model for mobile user motion is explained. The noise and uncertainty sources in the VLC system and their effect on the system are examined. Finally, possible contributions of this study are discussed.

4.1 The Kalman Filter

Kalman filter is a powerful mathematical tool for stochastic estimation of noisy measurements. It is a recursive solution for the discrete-linear time data filtering problem [31]. The filter has two steps: predict and correct. The process evolves according to a linear stochastic difference equation, and measurements are given as

$$\mathbf{x}_k = A\mathbf{x}_{k-1} + Bu_k + \mathbf{w}_{k-1}, \tag{4.1}$$

$$\mathbf{z}_k = H\mathbf{x}_k + \mathbf{v}_k, \tag{4.2}$$

where $\mathbf{x} \in \mathbb{R}^n$ denotes the state of the process, and $\mathbf{z} \in \mathbb{R}^m$ is the observation of the state. A is an $n \times n$ matrix that drives the state from time $k-1$ to k. B is $n \times l$ is the control input matrix that relates to control input $\mathbf{u} \in \mathbb{R}^l$. H is $m \times n$ measurement matrix. $\mathbf{w}_{k-1}$ and $\mathbf{v}_k$ are the random noise for process and measurement, respectively. For optimality to hold, they must be normally distributed and independent of each other.

$$p(\mathbf{w}_{k-1}) \sim N(0, Q_{k-1}), \tag{4.3}$$

$$p(\mathbf{v}_k) \sim N(0, R_k). \tag{4.4}$$

$Q_{k-1} = \mathbb{E}[\mathbf{w}_{k-1}\mathbf{w}_{k-1}^T]$ is the process noise covariance matrix, and $R_k = \mathbb{E}[\mathbf{v}_k\mathbf{v}_k^T]$ is the measurement noise covariance matrix.

The mean square value of the estimation error is minimized in Kalman filtering. The objective function to be minimized is $\mathbb{E}(\mathbf{x}_k - \hat{\mathbf{x}}_k)^2$, where $\hat{\mathbf{x}}_k$ is the estimate of the state. This is equal to minimizing the sum of diagonal elements of the error covariance matrix of the estimate,

$$\mathbf{P}_{k|k} = \mathbb{E}[(\mathbf{x}_k - \hat{\mathbf{x}}_{k|k})(\mathbf{x}_k - \hat{\mathbf{x}}_{k|k})^T]. \tag{4.5}$$

In this study, $\mathbf{x}$ and $\mathbf{z}$ denotes states and measurements vectors, respectively. For one time step k, the states $\mathbf{x}_k$ are the position and velocity of the mobile user that is according to a piecewise constant velocity model and the measurement $\mathbf{z}_k$ is the RSS that depends on the user position and the angles between the source and receiver. Since the measurement function is nonlinear, it is defined by (4.6) instead of (4.2)

$$\mathbf{z}_k = h_k(\mathbf{x}_k) + \mathbf{v}_k \tag{4.6}$$

When Gaussianity conditions are violated, the KF still solve for the least–squares sequential solution.

4.1.1 Derivation of Kalman Filter

The Kalman filter recursion can be described in two steps. The initial conditions of states $\mathbf{x}_0$ and covariance $\mathbf{P}_0$ are chosen according to previously known properties of the states.

We let $\hat{\mathbf{x}}_{k|k-1}$ represent the *a priori* state estimate at step k given the information about the process prior to step k, and $\hat{\mathbf{x}}_k$ represents the *a posteriori* state estimate at step k given measurement $\mathbf{z}_k$. The related errors and their covariances are defined as

$$\mathbf{e}_{k|k-1} = \mathbf{x}_k - \hat{\mathbf{x}}_{k|k-1}, \tag{4.7}$$

$$\mathbf{e}_k = \mathbf{x}_k - \hat{\mathbf{x}}_k, \tag{4.8}$$

$$\mathbf{P}_{k|k-1} = \mathbb{E}[\mathbf{e}_{k|k-1}\mathbf{e}_{k|k-1}^T], \tag{4.9}$$

$$\mathbf{P}_k = \mathbb{E}[\mathbf{e}_k\mathbf{e}_k^T]. \tag{4.10}$$

The objective of Kalman filter is to find the maximum *a posteriori* (MAP) estimate of the state as a linear combination of an *a priori* estimate and a weighted difference between an actual measurement and a measurement prediction. The correction function is given as

$$\hat{\mathbf{x}}_k = \hat{\mathbf{x}}_{k|k-1} + \mathbf{K}_k(\mathbf{z}_k - H\hat{\mathbf{x}}_{k|k-1}). \tag{4.11}$$

$\mathbf{K}$ is the $n \times m$ the Kalman gain matrix that minimizes the a posteriori error covariance. Furthermore, if the measurement error covariance R approaches zero, the gain depends on the residual; if the a priori estimate error covariance $\mathbf{P}_{k|k-1}$ approaches zero, the gain goes to zero:

$$\mathbf{K}_k = \mathbf{P}_{k|k-1} H^T (H \mathbf{P}_{k|k-1} H^T + R)^{-1} \tag{4.12}$$

The most important points are;

- As $R \to 0$, the measurement $\mathbf{z}_k$ is trusted more than the predicted measurement $H\hat{\mathbf{x}}_{k|k-1}$,
- As $P \to 0$, $H\hat{\mathbf{x}}_{k|k-1}$ is trusted more than $\mathbf{z}_k$ [32].

$(\mathbf{z}_k - H\hat{\mathbf{x}}_{k|k-1})$ is the measurement innovation which shows the difference between the predicted measurement and the actual measurement. In this study, A is the

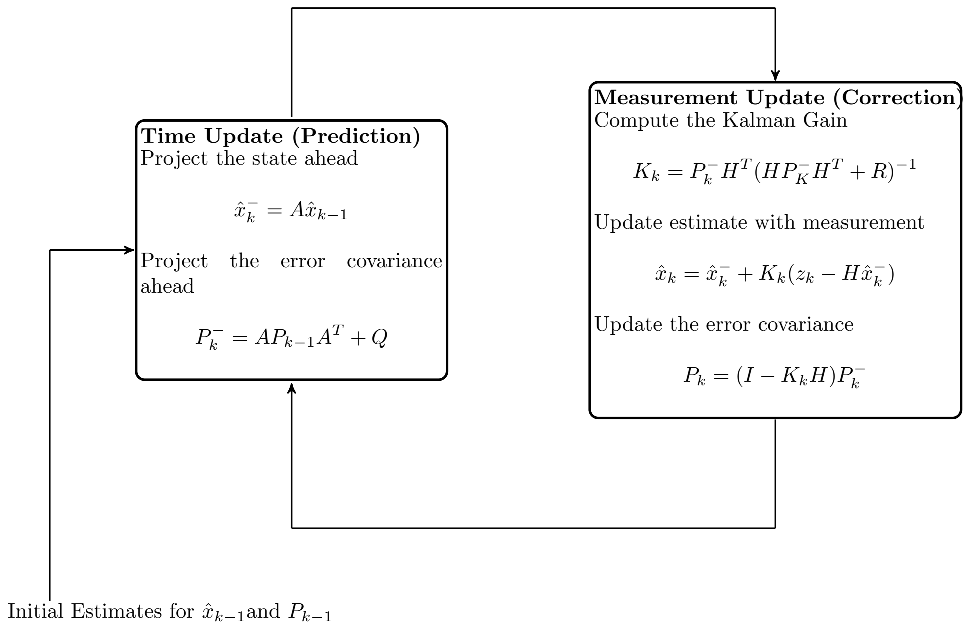

Figure 4.1: Kalman filter recursion.

kinematic motion model of the user, $\mathbf{x}$ is the state of the user, position and velocity in x and y directions. $\mathbf{z}_k$ is the RSS measurements from each lamp. In this study, there are four lamps in the room. Each lamp is coded with orthogonal codes. So the receiver can distinguish and measure the optical power intensity from all of the lamps. The measurement vector is denoted by,

$$\mathbf{z}_k = \begin{pmatrix} RSS_{Lamp1} \\ RSS_{Lamp2} \\ RSS_{Lamp3} \\ RSS_{Lamp4} \end{pmatrix} + \mathbf{v}_k \tag{4.13}$$

4.1.2 The Extended Kalman Filter (EKF)

The process or the measurements are not linear in many applications. The extended Kalman filter is an approach where nonlinearities are linearized at the current estimate. Given below are a nonlinear stochastic difference equation and a set of nonlinear measurements, respectively

$$\mathbf{x}_k = f(\mathbf{x}_{k-1}, \mathbf{w}_{k-1}) \tag{4.14}$$

$$\mathbf{z}_k = h(\mathbf{x}_k) + \mathbf{v}_k \tag{4.15}$$

The variables denote the same as in Section 4.1. The linearization process is carried out by calculating the Jacobian matrices of A, H, respectively.

$$A_{[i,j]} = \frac{\delta f_{[i]}}{\delta x_{[j]}}(\hat{\mathbf{x}}_{k-1}), \tag{4.16}$$

$$H_{[i,j]} = \frac{\delta h_{[i]}}{\delta x_{[j]}}(\tilde{\mathbf{x}}_{k-1}). \tag{4.17}$$

$\tilde{x}$ is an approximation of state without w in (4.12).

$$\hat{\mathbf{x}}_k^- = f(\hat{\mathbf{x}}_{k-1}) \tag{4.18}$$

$$\mathbf{P}_k^- = A_k \mathbf{P}_{k-1} A_k^T + \mathbf{W}_k Q_{k-1} \mathbf{W}_k^T \tag{4.19}$$

$$K_k = P_k^- H_k^T (H_k \mathbf{P}_k^- H_K^T + \mathbf{V}_k R_k \mathbf{V}_k^T)^{-1} \tag{4.20}$$

$$\hat{\mathbf{x}}_k = \hat{\mathbf{x}}_k^- + K_k(\mathbf{z}_k - h(\hat{\mathbf{x}}_k^-)) \tag{4.21}$$

$$\mathbf{P}_k = (I - K_k H_k)\mathbf{P}_k^- \tag{4.22}$$

The EKF recursions are given in (4.18)–(4.22). The EKF has some serious limitations in application, since it depends on the linearization of nonlinear functions. Calculations of the Jacobians are not easy and prone to errors. Furthermore, the Jacobian matrices must exist and the error propagation must be able to be represented by a linear or a quadratic function.

The VLC channel equation given in (2.7) is a nonlinear function. As a result, the measurements are nonlinear. EKF relies on the linearization of nonlinear functions. The derivative of the channel equation is hard to evaluate without angle information. So H is difficult to define.

In our problem, we calculate the derivatives using the finite difference method for linearization. This method is a generalized and flexible approach. The algorithm consists of an online phase and an offline phase. In the offline phase the expected power distribution in the room is calculated. The grid in Figure 4.2 represents the expected power distribution matrix $\mathbf{P} = [P_{i,j}]$, where $i = 1, \ldots, N$ and $j = 1, \ldots, J$ are the dimensions of the room. The dimension of the room is divided by N or J, that sets the grid resolution in centimeters or decimeters. We calculate the predicted state $\hat{\mathbf{x}}$, and it is represented by $\star$. We take the RSS in this grid as the predicted power $\hat{\mathbf{P}}(\hat{\mathbf{x}})$. Finally, we calculate the difference between the upper $P_{(i,j-1)}$, down $P_{(i,j+1)}$, left $P_{(i-1,j)}$ and $P_{(i+1,j)}$ grids.

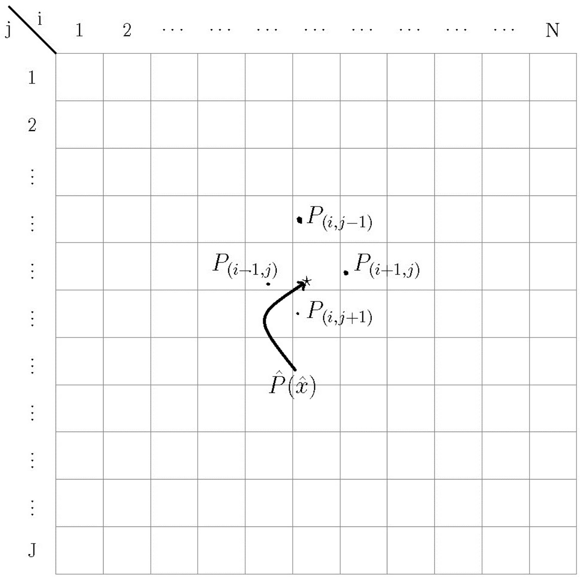

Figure 4.2: The power distribution matrix.

$$H(\mathbf{x}) \approx \begin{bmatrix} \frac{P_{i+1,j}-P_{i-1,j}}{\Delta x} & \frac{P_{i1,j+1}-P_{i,j-1}}{\Delta x} \end{bmatrix}. \tag{4.23}$$

where i and j is the indices of the power of the predicted state vector, and Δx_j is the granularity of the power map. In (4.21), we replace $h(\hat{\mathbf{x}}_k^-)$ with the predicted RSS which depends on the predicted position $H\mathbf{x}_k^-$.

4.2 Dynamic Model for Mobile User Motion

The success of the Kalman filter depends on the choice of the dynamic model. The previous studies on human motion modeling showed that one of the best models is the piecewise constant white acceleration model [33].

The mobile user is assumed to be moving in a Cartesian coordinate system. The state is $\mathbf{x}_k = [x_k \quad y_k \quad \dot{x}_k \quad \dot{y}_k]^T$. The transition matrix and the covariance of process noise of a piecewise constant acceleration motion is given below, where $\mathbf{w}$ is zero mean normal distributed noise with covariance $\mathbb{E} = [\mathbf{w}_{k-1}\mathbf{w}_{k-1}^T]$ and v is the spectral density of the noise [32],

$$\mathbf{x}_k = \begin{pmatrix} x_k \\ y_k \\ \dot{x}_k \\ \dot{y}_k \end{pmatrix} = \begin{pmatrix} 1 & 0 & \Delta t & 0 \\ 0 & 1 & 0 & \Delta t \\ 0 & 0 & 1 & 0 \\ 0 & 0 & 0 & 1 \end{pmatrix} \begin{pmatrix} x_{k-1} \\ y_{k-1} \\ \dot{x}_{k-1} \\ \dot{y}_{k-1} \end{pmatrix} + \mathbf{w}_{k-1}, \tag{4.24}$$

$$\mathbb{E}[\mathbf{v}_{k-1}\mathbf{v}_{k-1}^T] = \begin{pmatrix} \frac{1}{3}\Delta t^3 & 0 & \frac{1}{2}\Delta t^2 & 0 \\ 0 & \frac{1}{3}\Delta t^3 & 0 & \frac{1}{2}\Delta t^2 \\ \frac{1}{2}\Delta t^2 & 0 & \Delta t & 0 \\ 0 & \frac{1}{2}\Delta t^2 & 0 & \Delta t \end{pmatrix} \sigma_v^2 \tag{4.25}$$

4.3 Signal-to-Noise Ratio Analysis and Uncertainties in the System

Signal-to-noise ratio (SNR) defines the quality of a sensor system. There are two main factors defining SNR on the receiver side, shot noise and thermal noise.

4.3.1 Shot Noise

Shot noise was first investigated by Schottky. It is caused by the random motions of electrons. When a photon falls on a photodiode, the generated current can be expressed as

$$I(t) = I_p + i_s(t), \tag{4.26}$$

$$I_p = RPr. \tag{4.27}$$

where I_p is the average current, R is the responsivity of the photodetector and Pr is the received power. $i_s(t)$ is the random current fluctuations. The spectral density of shot noise is constant and $S_s(f) = qI_p$. The shot noise variance is [34]

$$\sigma_s^2 = \mathbf{R}(i_s^2(t)) = \int_{-\infty}^{\infty} qI_p \mathrm{d}f = 2qI_p\Delta f. \tag{4.28}$$

The dark current I_d is also a contributing factor in the shot noise. If we add dark current I_d and rewrite the shot noise variance,

$$\sigma_{shot}^2 = 2q(I_p + I_d)\Delta f = 2qRP_{in}B + 2qI_{bg}I_2B, \tag{4.29}$$

q is the electronic charge, B is the modulation bandwidth, I_{bg} is the background current, I_2 the noise bandwidth factor. P_{in} is given as

$$P_{in} = \sum_{i=1}^{\mathrm{n}} H_i(0)P_i, \tag{4.30}$$

n is the number LEDs in the room, $H_i(0)$ is the LOS channel gain and P_i is the instantaneous emitted power from ith LED.

4.3.2 Thermal Noise

The random motion of electrons in a conductor generates a current. It is independent of voltage. It depends on the absolute temperature [34]. Rewriting (4.25)

$$I(t) = I_p + i_s(t) + i_T(t), \tag{4.31}$$

$i_T(t)$ is the thermal noise and its variance is given as [8]

$$\sigma_{thermal}^2 = \frac{8\pi kT_K}{G_0}\eta AI_2B^2 + \frac{16\pi^2 kT_K\Gamma}{g_m}\eta^2 I_3B^3 \tag{4.32}$$

k is Boltzmann's constant, T_K is the temperature in Kelvin, G_0 is the open loop voltage gain, η is the capacitance of photodetector, Γ is the FET channel noise factor, g_m is the FET transconductance and $I_3 = 0.0868$.

4.3.3 Uncertainties in the System

Shot and thermal noises are effectively on the receiver side. However, in a real system, there are other uncertainties that degrade the SNR. In this study, these uncertainties are addressed as additional measurement noise. These may be caused by

- Blocking of LOS
- Shadowing effects
- Random changes on the tilt angle of the mobile device
- The lay-out of the room
- Changes in the average power distribution map.

4.3.4 Signal to Noise Ratio

Signal to noise ratio is calculated when shot, thermal and uncertainty noises are present in the system. The SNR is given as

$$SNR = \frac{R^2 P_r^2}{\sigma_{shot}^2 + \sigma_{thermal}^2 + \sigma_{uncertainty}^2} \tag{4.33}$$

Figure 4.3 shows the SNR levels for the deterministic 25-LED lamp positioned at (3.75, 3.75, 3) m.

Table 4.1: Shot and Thermal Noise Parameters

Parameter	Value
Electron Charge, q	$1.602 * 10^{-19} C$
PD Responsivity, R	$0.54\ A/W$
Total Received Power, P_{rectot}	$\sum_{i=1}^{N} H_{LOS_i} P_i$
Noise Bandwidth, B	$640\ KHz$
Background Current, I_{bg}	$740 \mu A$ indirect sunlight $5100 \mu A$ direct sunlight
Noise Bandwidth Factor, I_2	0.562
Boltzmann's Constant, k	$1.3806488 * 10^{-23}$
Absolute Temperature, T_k	$295\ K$
I_3	0.0868
FET channel noise factor, Γ	1.5
Capacitance of PD, μ	$112\ pF/cm^2$
Open loop gain, G_0	10
Fet transconductance, g_m	$30\ mS$
Photo detector area, A	$1\ cm^2$
Room dimension $(x \times y \times z)$	$5\ m \times 5\ m \times 3\ m$
Transmitted power	max. $25 * 20\ mW/bulb$
Codes used by LED bulbs	$\begin{pmatrix} 1 & 0 & 0 & 0 \\ 0 & 1 & 0 & 0 \\ 0 & 0 & 1 & 0 \\ 0 & 0 & 0 & 1 \end{pmatrix}$
Field of view Ψ_c	$70°$
Optical filter gain	1.0
Refractive index of opt. concentrator	1.5

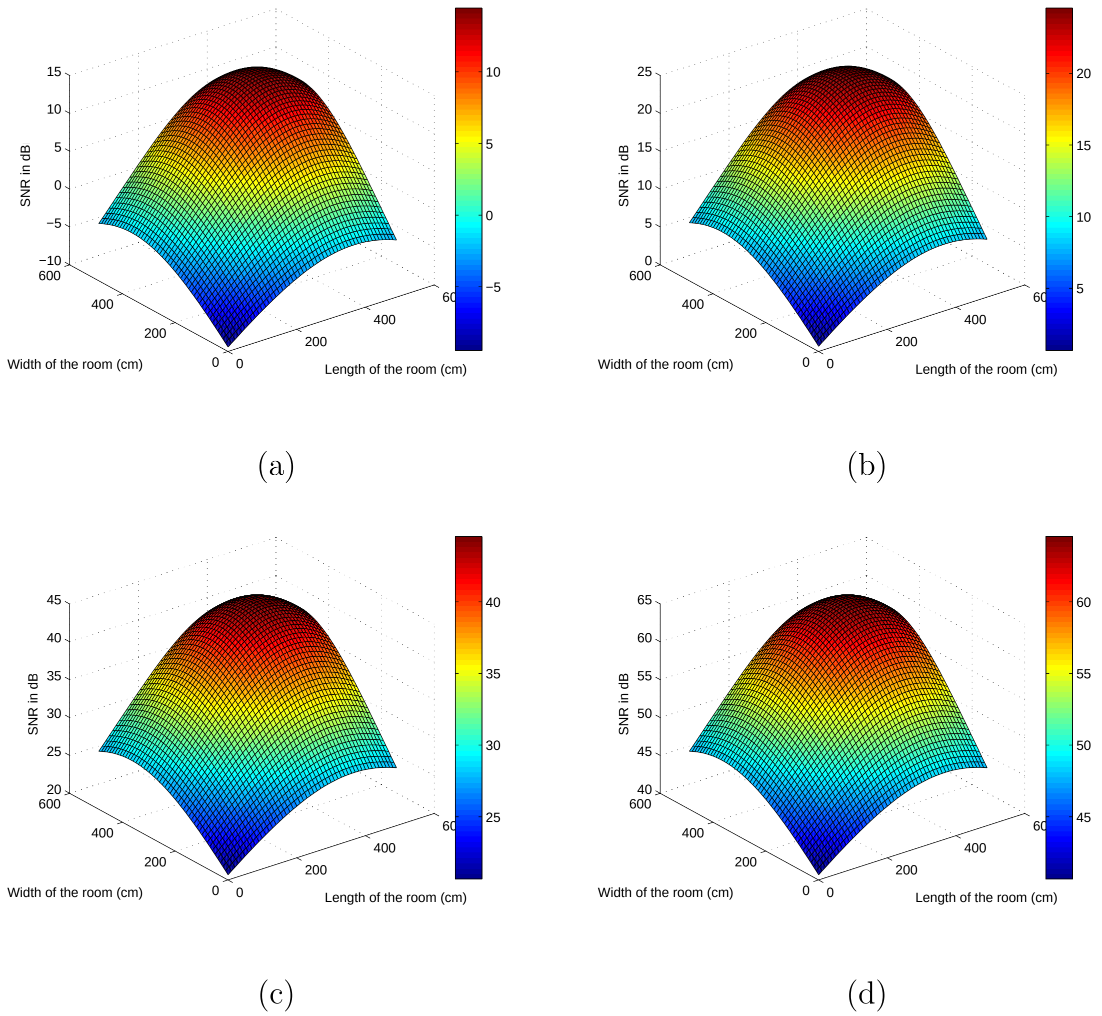

(a) (b) (c) (d)

Figure 4.3: Signal-to-noise ratio, (a) 15 dB, (b) 25 dB, (c) 45 dB , (d) 65 dB.

4.4 Average Floor Map

The diffusing lamp model is assumed to be slowly time varying like the movements of the crystal prisms on a chandelier. The movement of the crystals causes changes in the power distribution map in the room slowly. We find the average power distribution map by averaging pre–defined time intervals. The room floor is divided into equal size sections using a rectangular grid. The power received in the each grid is computed as the average expected power over the area of the rectangular portion of the floor. The best update frequency depends on the air flow or the interference of light with the moving people in the room. Later on, this averaged power distribution is provided to the mobile user.

4.5 Implementation of Method

The extended Kalman filter is implemented on an empty room with dimension of $5 \times 5 \times 3$ m^3. There are four lamps on the ceiling. Each lamp has 25 LEDs. The performance evaluation criterion is the root mean squared error (RMSE). The uncertainties mentioned in Section 4.3.3, may change the SNR, and the thermal and the shot noises are not enough to model the noise in the system.

The room is divided into equal size grids. The receiver area is assumed as one grid position. There are two grid resolutions tested in this study. Grid areas are 1 cm^2 or 1 dm^2. The states x and y are the Cartesian positions and $\dot{x}$ and $\dot{y}$ are the velocities. We assume that the mobile user speed is 10 cm/sec in the x direction and 30 cm/sec in the y direction.

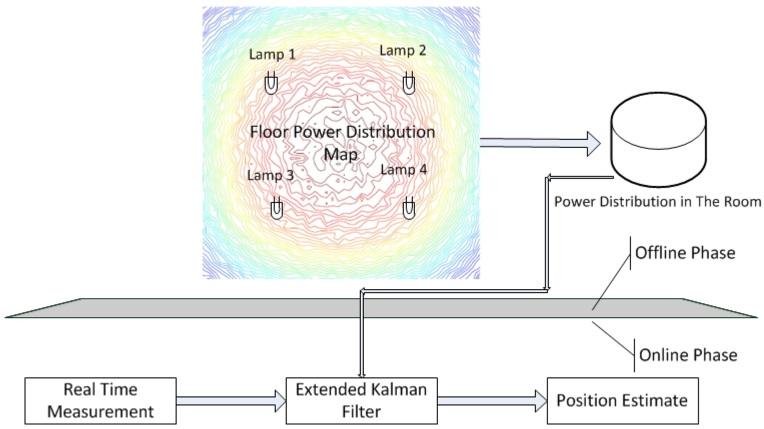

Figure 4.4: Positioning method process by EKF in Visible Light Positioning (VLP) system.

Figure 4.4 shows the positioning method, the power distribution on the room floor is collected in the offline phase. The online phase measurements and the power distribution map are combined in the online phase.

Angulation and lateration methods are commonly used. Almost every study cited in the literature review section uses trilateration for positioning. However, angulation and lateration is susceptible to the noise, and the positioning error gets bigger as the uncertainty in the system increases. We also compare the performance of the trilateration method with the Kalman method.

In the trilateration method, it is assumed that the LEDs are facing downwards and the geometry between the lamp and the receiver is known. This is not true when a diffuser is used. We cannot model the geometry of refraction of light through a diffuser. It is a random process. That is why we argue that one cannot use the trilateration method for a diffusing lamp and obtain accurate positioning.

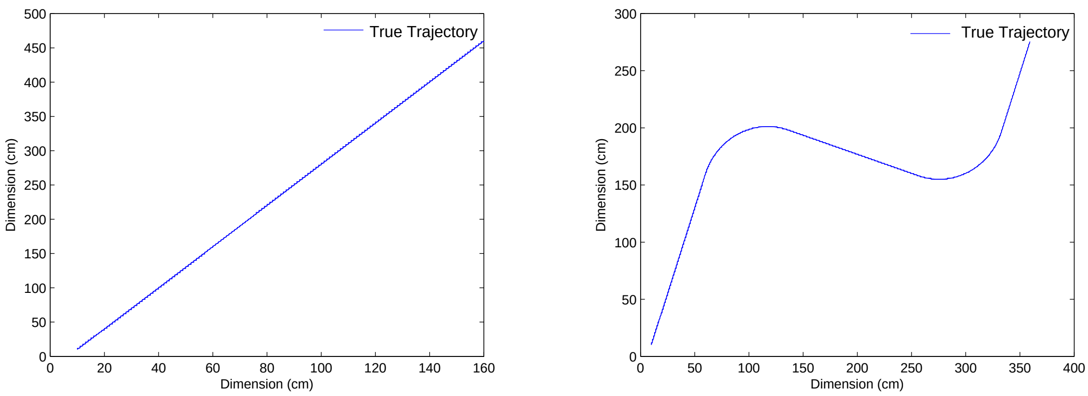

(a) (b)

Figure 4.5: Mobile user true trajectory, (a) Straight motion, (b) S–shaped motion.

The performance of the proposed method is evaluated for two kinds of trajectories: a non-linear trajectory which we call ‘S–shaped’ and a linear trajectory called ‘Straight’. Figure 4.5 shows the true trajectories.

4.5.1 Kalman Filter Tuning

The Kalman filter's performance depends on an accurate description of the process and its noise. In general, before implementation, an optimal process noise covariance R can be found. The process noise covariance Q is harder to obtain, because we cannot observe the process that is estimated. The simple model with a measurement noise covariance R gives accurate results as the measurements are reliable.

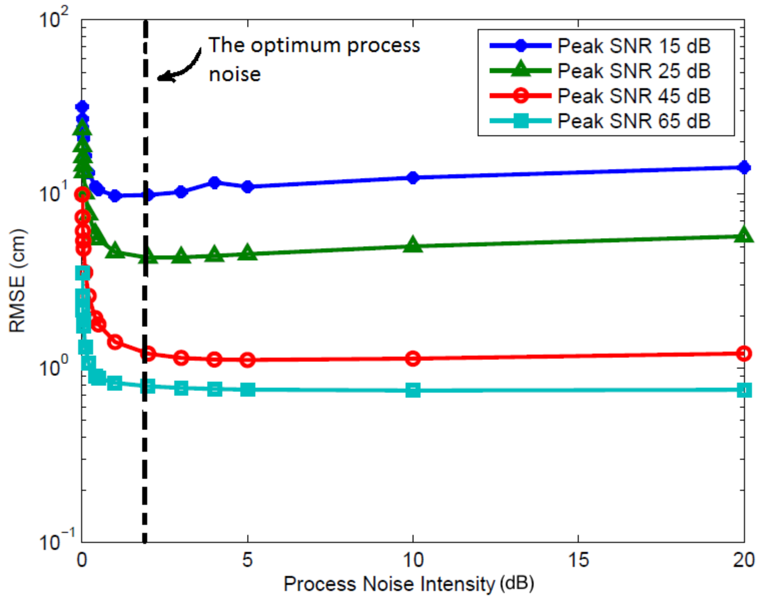

Figure 4.6: Root mean square of positioning error for the deterministic 25-LED lamp with LED semiangle 60° using EKF.

Figure 4.6 shows the effect of the choice of process noise on the RMSE. We simulated the model and ran the EKF for different SNR levels. For different SNR levels the optimum value of the process noise we should use is the minimum point of the curves.

4.5.2 Results

The tracking results for different SNR levels are shown in this section. The initial position is chosen with reference to a known point like a door, window or light source. The initial position error in the error covariance matrix is chosen as 30 centimeters away from this point and the initial velocity error may not exceed the velocity of the mobile user. The initial state and initial error covariance are given as:

$$\mathbf{x}_0 = [30\;30\;10\;30]^T, \tag{4.34}$$

$$\mathbf{P}_0 = \begin{pmatrix} 50 & 0 & 0 & 0 \\ 0 & 50 & 0 & 0 \\ 0 & 0 & 10 & 0 \\ 0 & 0 & 0 & 30 \end{pmatrix} \tag{4.35}$$

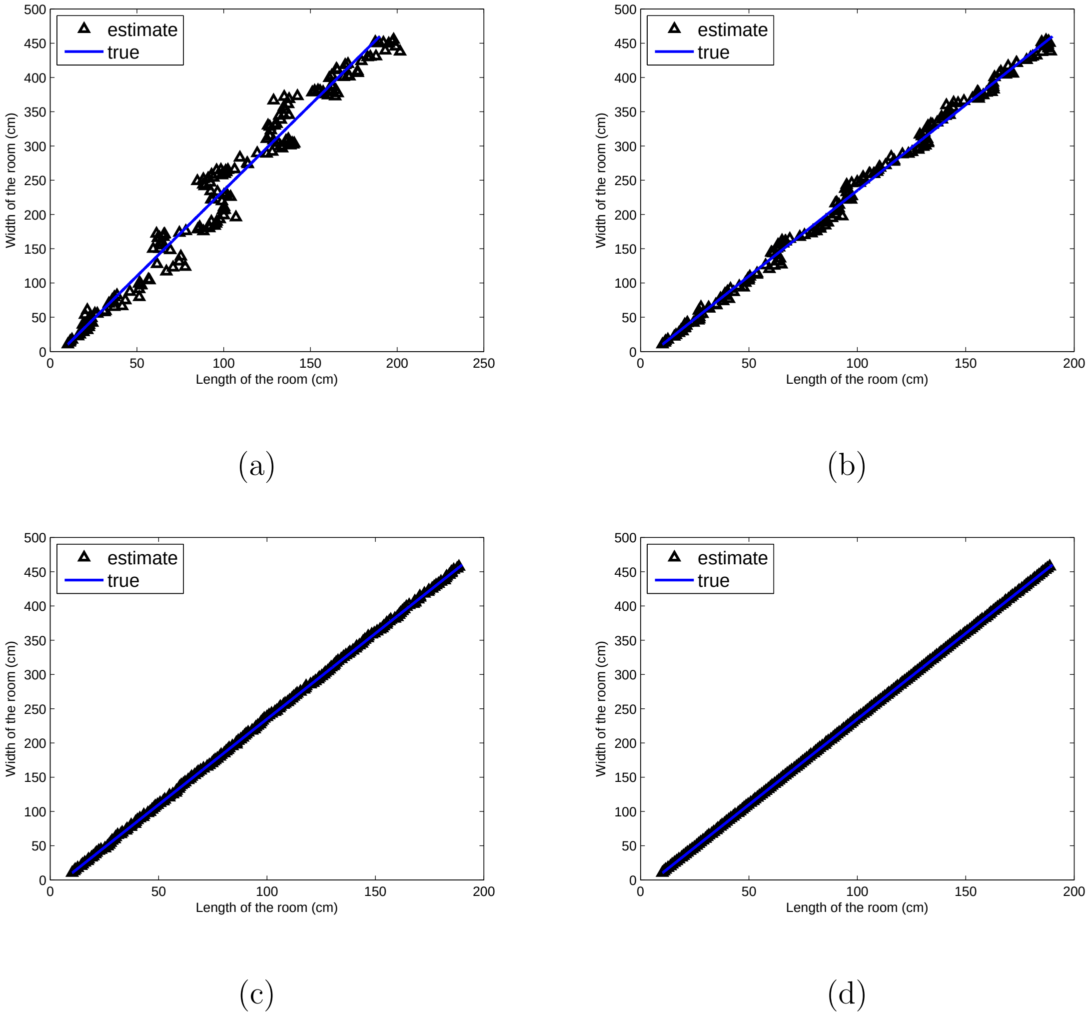

(a) (b) (c) (d)

Figure 4.7: Tracking results of a linear trajectory when the deterministic 25-LED lamp is used for SNR, (a) 15 dB, (b) 25 dB, (c) 45 dB, (d) 65 dB.

Figure 4.7 shows tracking results for a mobile user following a straight trajectory when the deterministic 25-LED lamp is used. The process noise and transmitted power from LEDs are kept the same for each scenario, but the measurement noise is changed. In the worst case scenario the SNR is 15 dB. Figure 4.7–(a) shows the tracking result for the worst case, where the RMSE is about 10 cm. As SNR increases, the filter trusts the measurement, and the RMSE decreases. Figure 4.7–(d) shows the best case scenario; The SNR is 65 dB and the RMSE is 0.6 cm.

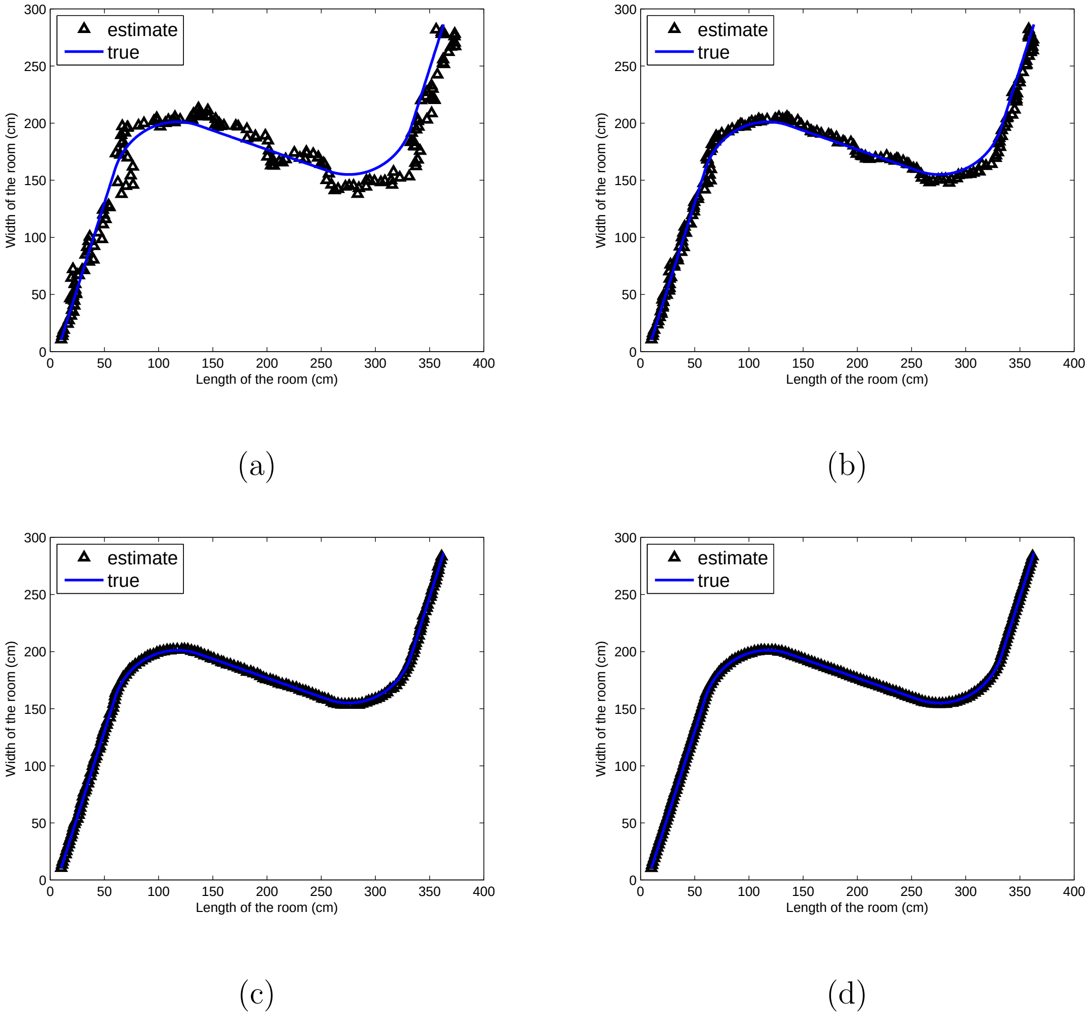

Figure 4.8: Tracking results of a S–shaped trajectory when the deterministic 25-LED lamp is used for SNR, (a) 15 dB, (b) 25 dB, (c) 45 dB, (d) 65 dB.

Figure 4.8 shows the tracking results for the S-shaped motion when the deterministic 25-LED lamp is used. The process noise and transmitted power from the LEDs are the same as for Figure 4.7. The results show the estimated trajectory for different noise levels. The worst case scenario RMSE is 10 cm and the best case scenario RMSE is 1 cm.

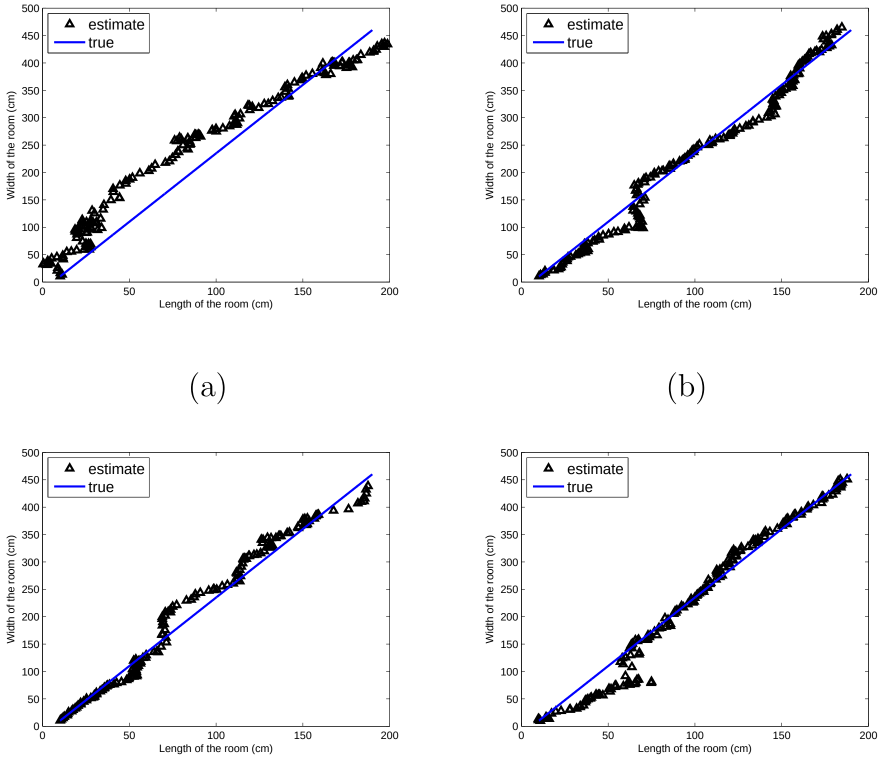

(a) (b)

(c) (d)

Figure 4.9: Tracking results of a linear trajectory when the diffusing lamp model is used for SNR, (a) 15 dB, (b) 25 dB, (c) 45 dB, (d) 65 dB.

The results for a diffusing lamp model are shown in Figure 4.9. The process noise and transmitted power from the LEDs are the same. The measurement noise is changed for each scenario. In the Figure 4.9–(a), the worst case scenario is shown, the RMSE in this case is 28 *cm*. The best case scenario shown in Figure 4.9–(d), the RMSE is 10 *cm*.

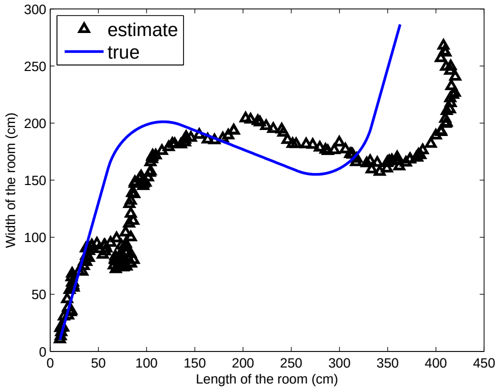

(a)

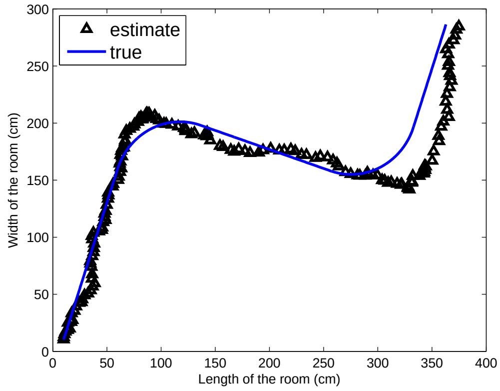

(b)

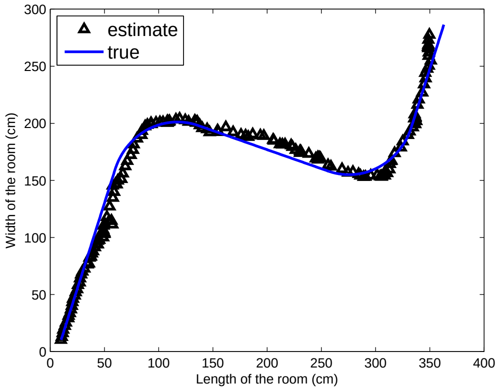

(c)

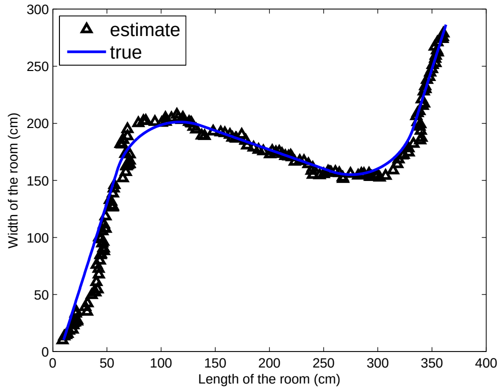

(d)

Figure 4.10: Tracking results of a S–shape trajectory when the diffusing lamp model is used for SNR, (a) 15 dB, (b) 25 dB, (c) 45 dB, (d) 65 dB.

The diffusing lamp model is used for the tracking result in Figure 4.10. The same conditions are present as the previous tracking results. The worst case scenario RMSE is 39 *cm* and the best case scenario RMSE is 11 *cm*.

The results from these experiments are summarized in Table 4.2. Although the results for a diffusing lamp model is worse than the deterministic lamp, the results are acceptable, in sense that in this study we assume that one human step is 30 *cm*.

Table 4.2: 95 % Confidence interval results for 100 Monte Carlo simulations

25-LED lamp S–shaped motion		25-LED lamp linear motion		Diffusing lamp S–shaped motion		Diffusing lamp linear motion	
SNR (dB)	RMSE (cm)	SNR (dB)	RMSE (cm)	SNR (dB)	RMSE (cm)	SNR (dB)	RMSE (cm)
15	9.8788	15	9.6664	15	38.8225	15	27.2620
25	4.3112	25	3.8284	25	32.9171	25	23.5954
45	1.2101	45	0.8942	45	23.9651	45	22.9732
65	0.7872	65	0.6323	65	10.4804	65	10.1293

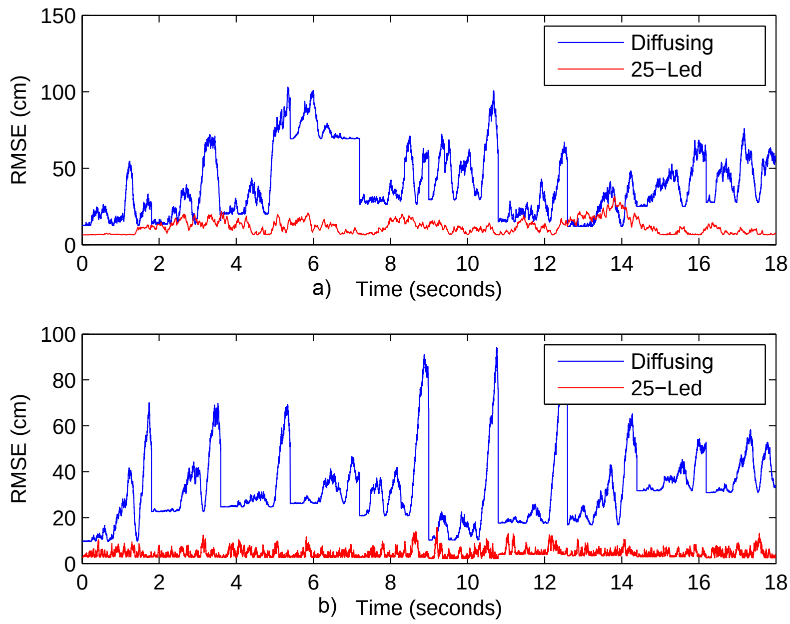

Figure 4.11: RMSE of position over time for SNR=15 dB (a) S–shaped motion, (b) Straight motion.

Figure 4.11–(a) shows the RMSE positioning error over time for S–shaped trajectory. Figure 4.11–(b) shows the RMSE positioning error for the straight trajectory. The results show that the positioning error is higher for the same noise and target motion when the diffusing lamp model is used. The error gets higher between fifth and eighth seconds and twelfth to fifteenth seconds. These are the time intervals where the mobile user starts the turning motion. Figures 4.12–4.14 show the positioning error for the S–shaped trajectory on subfigure (a) and the linear

trajectory in the subfigure (b). The same conclusions can be made for different SNR.

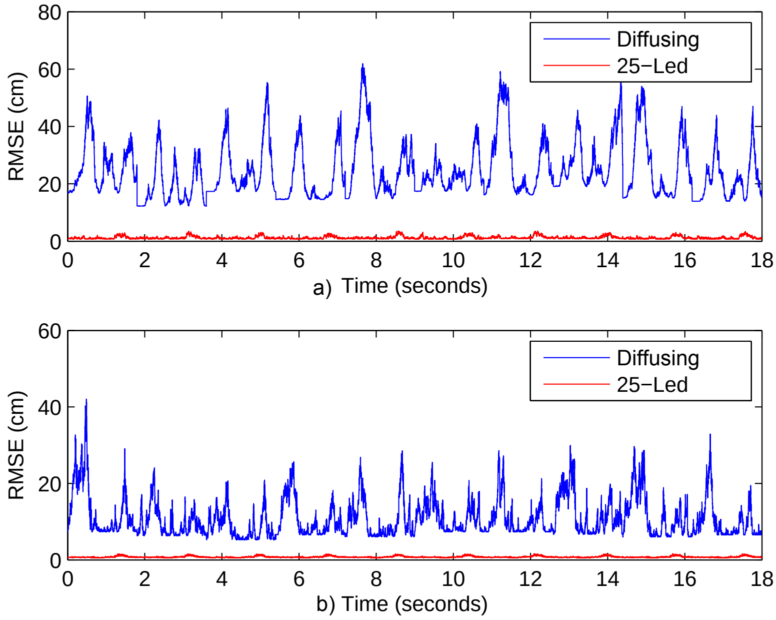

Figure 4.12: RMSE of position over time for SNR=25 dB (a) S–shaped motion, (b) Straight motion.

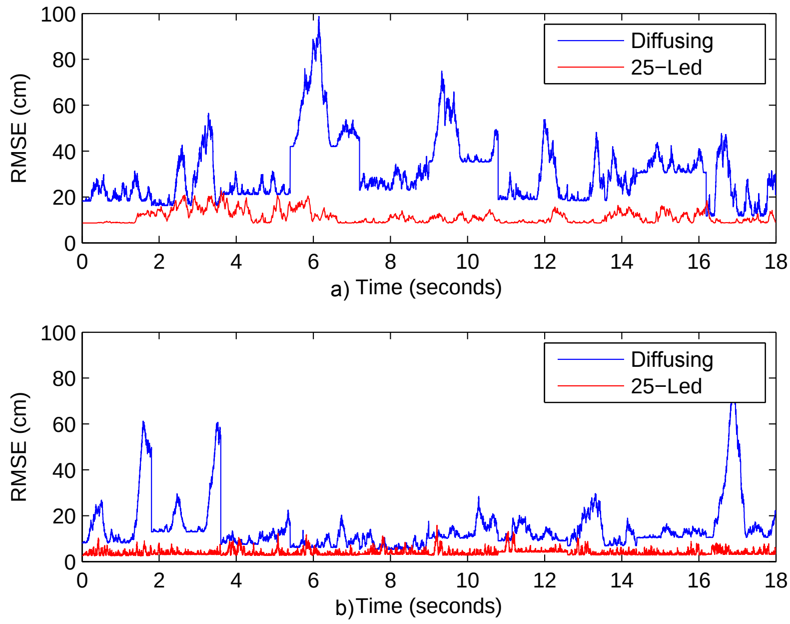

Figure 4.13: RMSE of position over time for SNR=45 dB (a) S–shaped motion, (b) Straight motion.

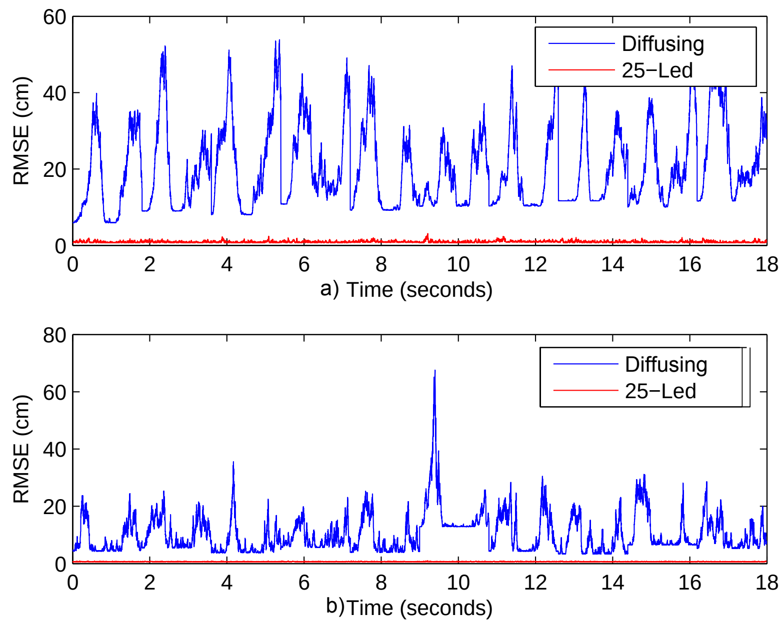

Figure 4.14: RMSE of position over time for SNR=65 dB (a) S–shaped motion, (b) Straight motion.

Figures 4.15–4.18 show the instantaneous position error of the deterministic and the diffusing lamp models for the motion models. The results show that the tracking performance of the deterministic 25–LED lamp is better than the random 25–LED lamp. This results from the fact that the finite difference between two RSS measurements for the random lamp is not as small as the deterministic lamp.

Figures 4.19–4.22 show the RMSE for velocity in x and y directions for the deterministic and the diffusing lamp models. The results show that as the SNR increases the tracking error decreases.

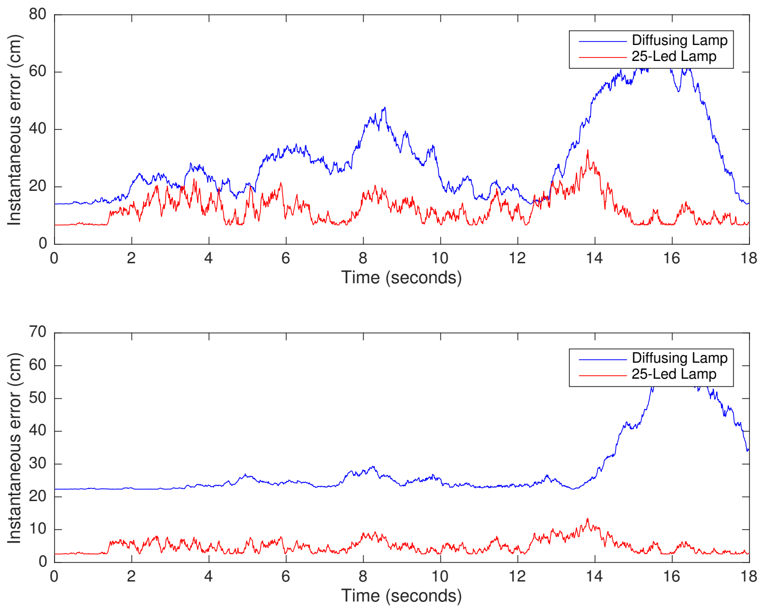

Figure 4.15: Instantaneous error of position over time for SNR=15 dB (a) S–shaped motion, (b) Straight motion.

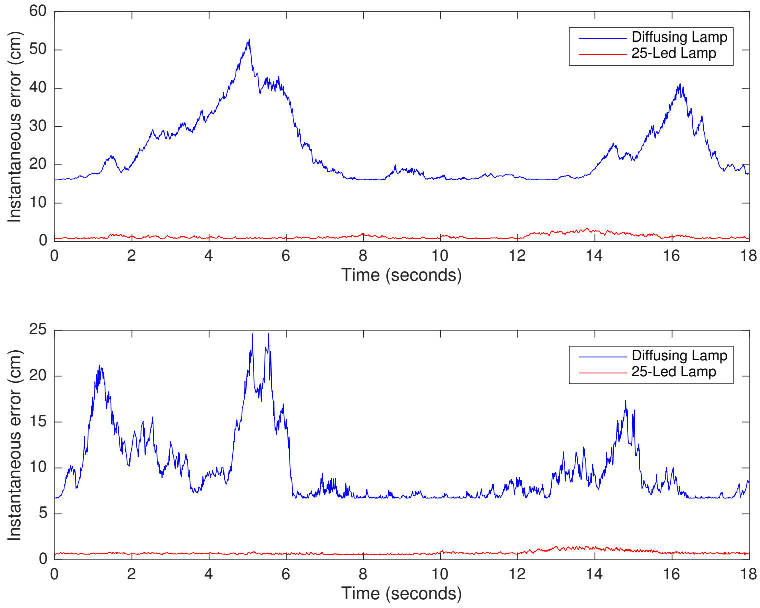

Figure 4.16: Instantaneous error of position over time for SNR=25 dB, (a) S–shaped motion, (b) Straight motion.

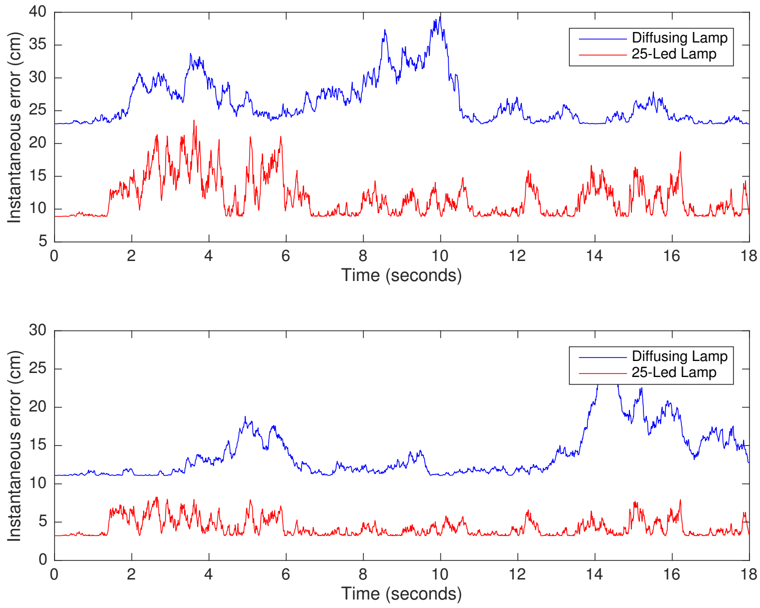

Figure 4.17: Instantaneous error over of position time for SNR=45 dB, (a) S–shaped motion, (b) Straight motion.

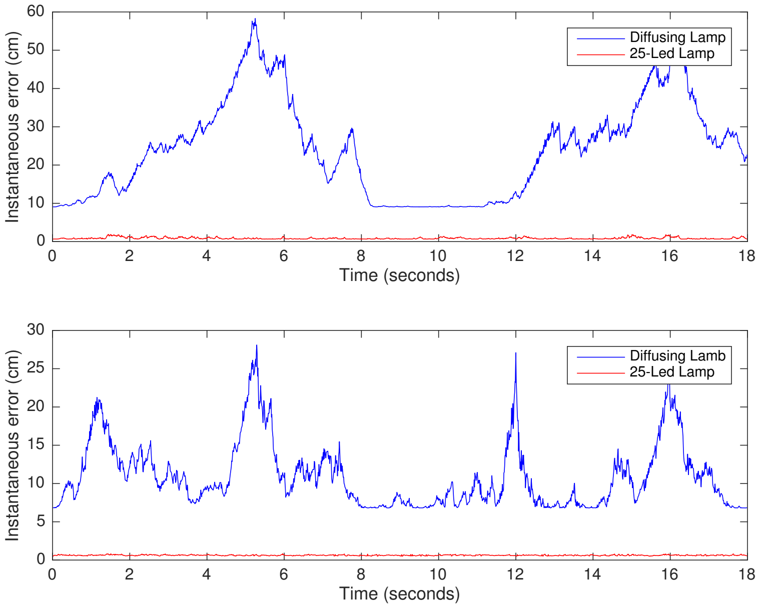

Figure 4.18: Instantaneous error over of position time for SNR=65 dB, (a) S–shaped motion, (b) Straight motion.

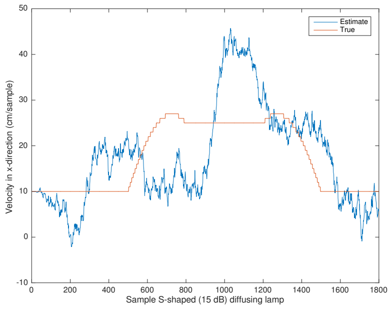

(a)

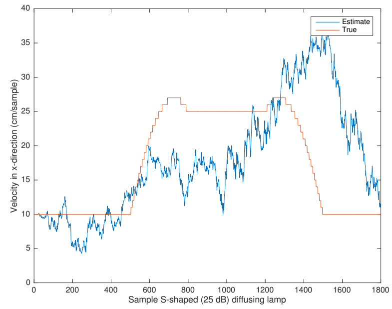

(b)

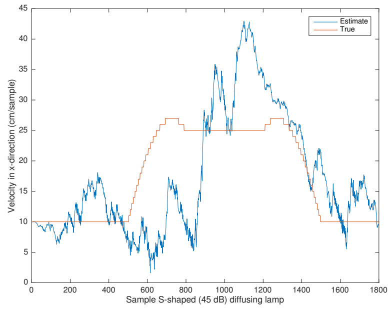

(c)

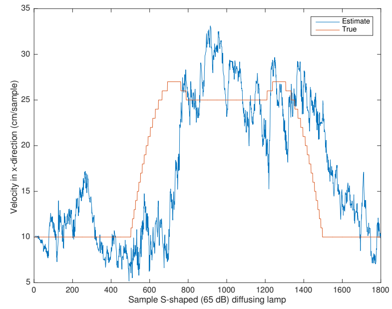

(d)

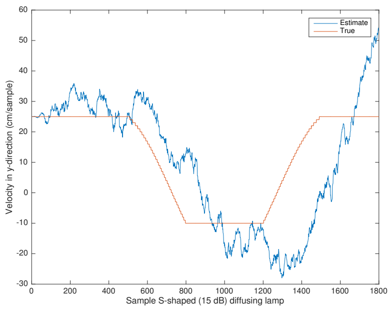

(e)

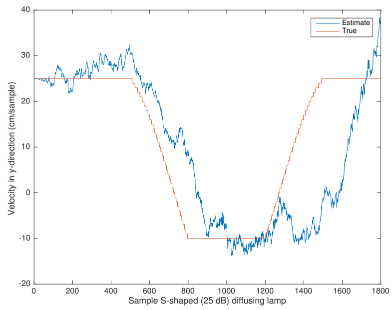

(f)

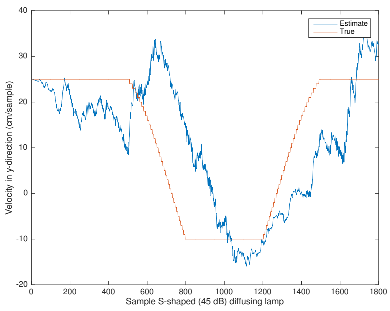

(g)

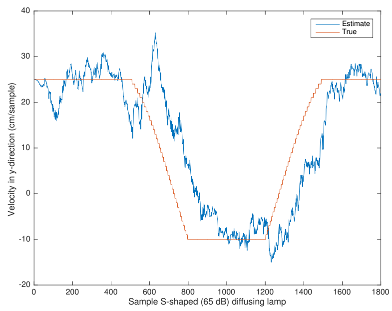

(h)

Figure 4.19: Velocity RMSE results of a S–shaped trajectory when the diffusing lamp model is used for SNR, (a) 15 dB, (b) 25 dB, (c) 45 dB, (d) 65 dB in x–direction and (a) 15 dB, (b) 25 dB, (c) 45 dB, (d) 65 dB in y–direction.

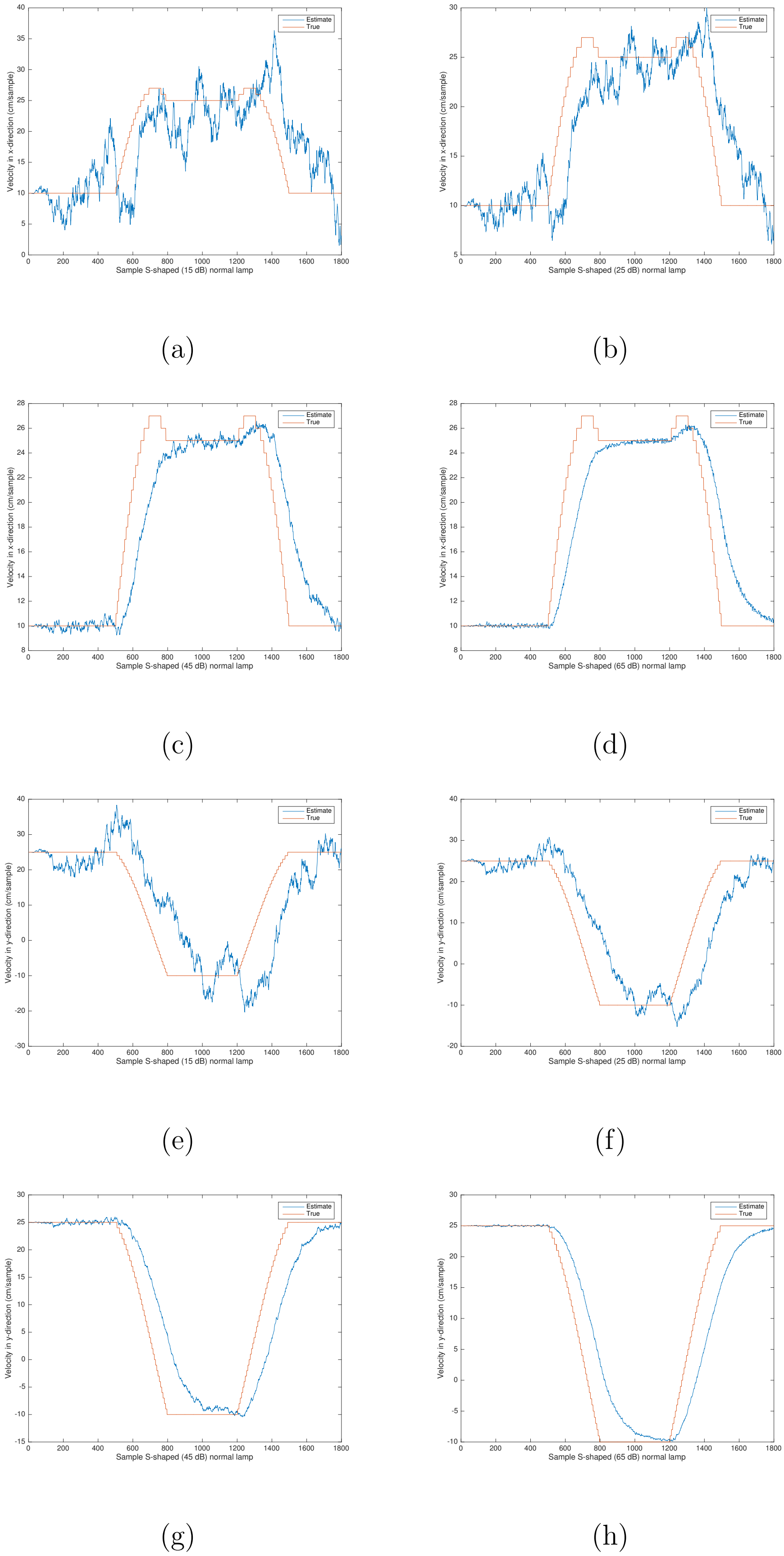

Figure 4.20: Velocity RMSE results of a S–shaped trajectory when the deterministic lamp model is used for SNR, (a) 15 dB, (b) 25 dB, (c) 45 dB, (d) 65 dB in x–direction and (a) 15 dB, (b) 25 dB, (c) 45 dB, (d) 65 dB in y–direction.

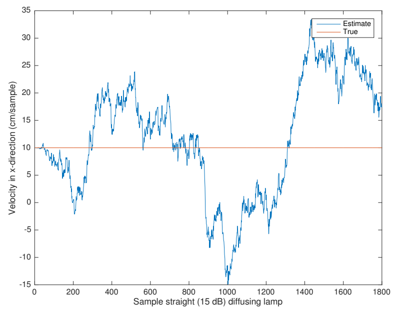

(a)

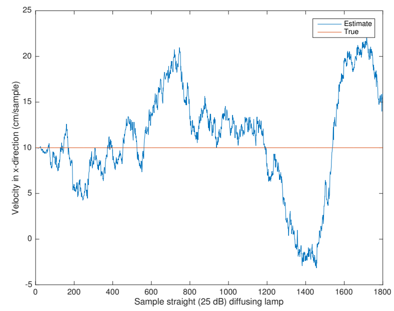

(b)

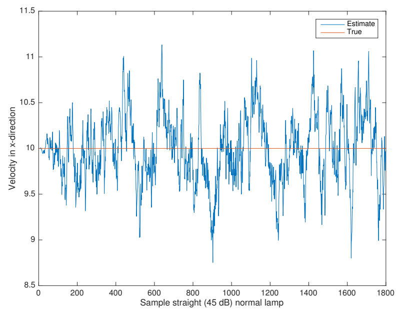

(c)

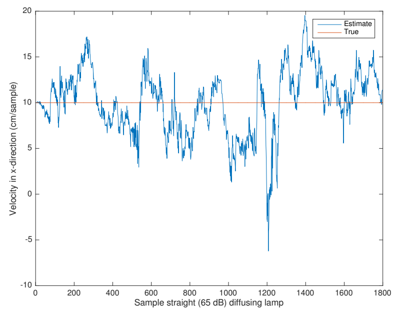

(d)

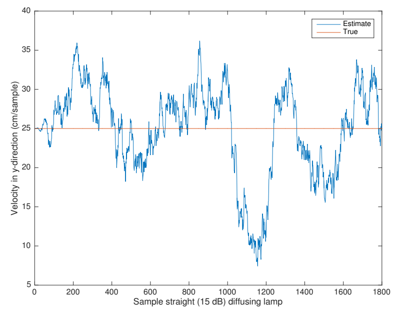

(e)

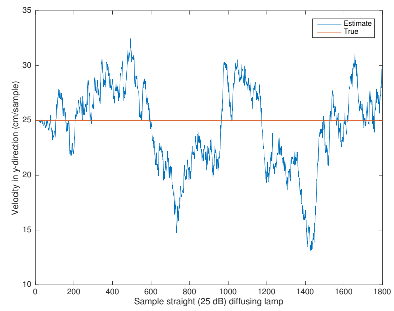

(f)

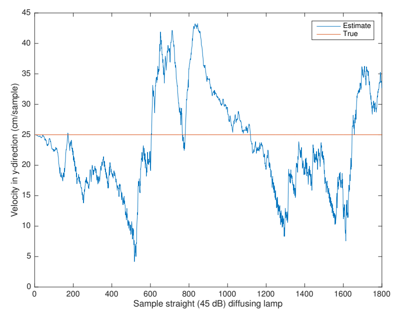

(g)

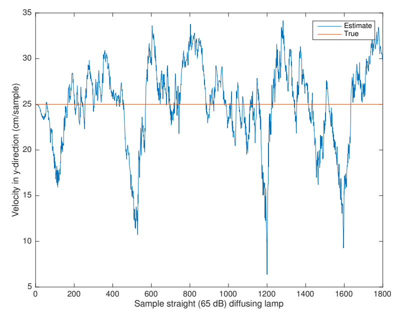

(h)

Figure 4.21: Velocity RMSE results of a straight trajectory when the diffusing lamp model is used for SNR, (a) 15 dB, (b) 25 dB, (c) 45 dB, (d) 65 dB in x–direction and (a) 15 dB, (b) 25 dB, (c) 45 dB, (d) 65 dB in y–direction.

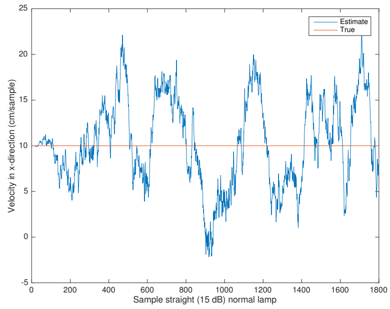

(a)

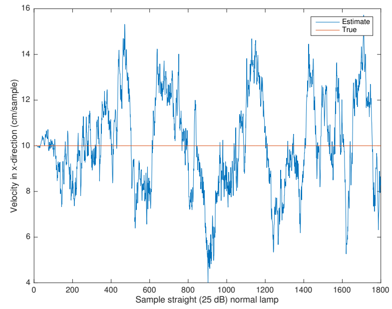

(b)

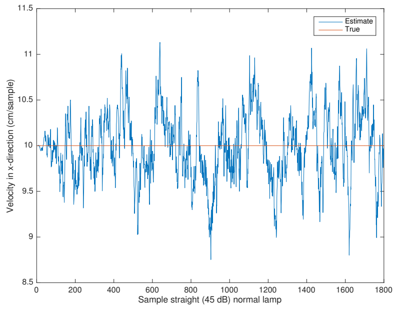

(c)

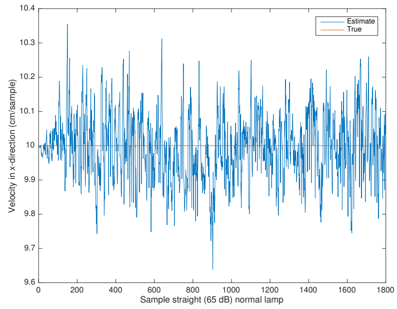

(d)

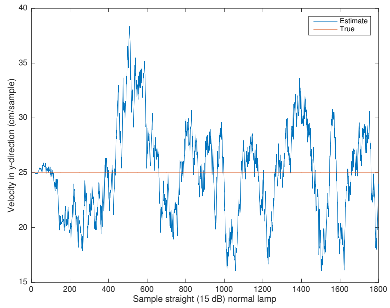

(e)

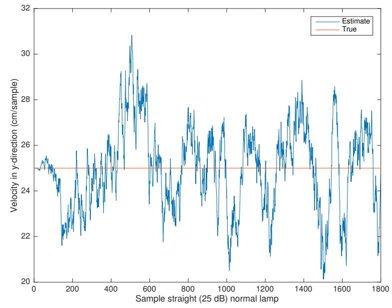

(f)

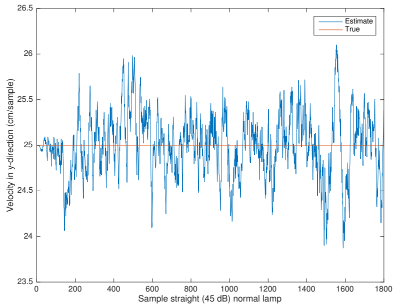

(g)

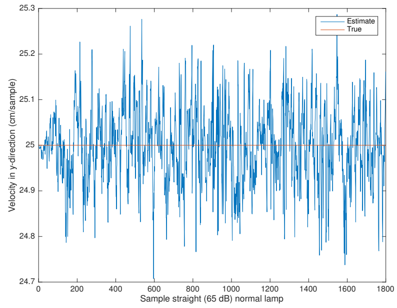

(h)

Figure 4.22: Velocity RMSE results of a straight trajectory when the deterministic lamp model is used for SNR, (a) 15 dB, (b) 25 dB, (c) 45 dB, (d) 65 dB in x–direction and (a) 15 dB, (b) 25 dB, (c) 45 dB, (d) 65 dB in y–direction.

4.5.3 Comparison of Trilateration and EKF Approaches

The performance comparison of trilateration and EKF approaches are presented in this section. Figure 4.23 gives the performance of trilateration and EKF methods. The room is divided into equal sized grids of 1 cm^2. The 25-LED lamp model has the lowest RMSE. The diffuser model is second compared to the trilateration method. The performance of trilateration depends on the channel propagation loss as discussed in Section 3.3.1. If we introduce noise to the channel then the RMSE increases for trilateration. The trilateration models are accurate when we take into account the thermal and shot noise. However, as discussed before this is not applicable to real life situations. The dynamics of the environment change almost every second if we think of a museum or a hotel lobby.

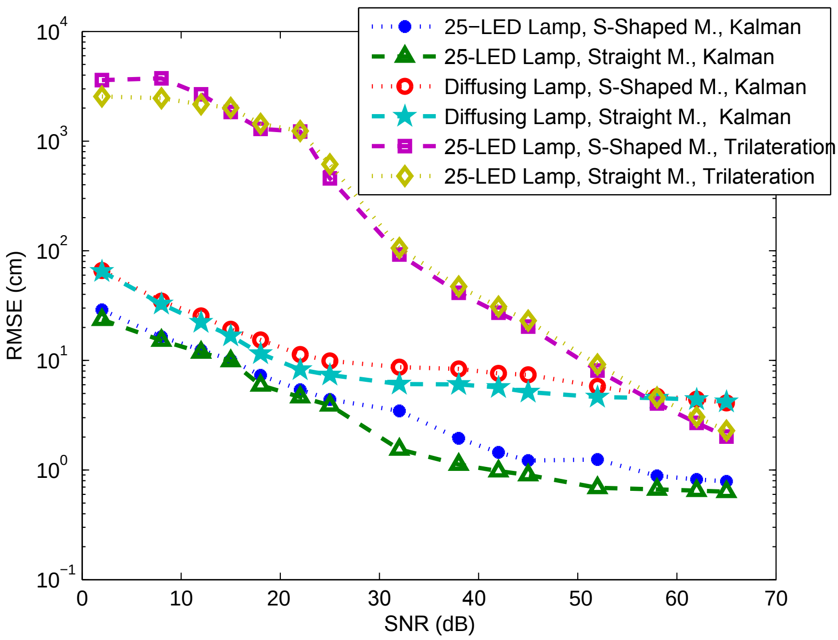

Figure 4.23: Comparison of trilateration and EKF when grid resolution is 1 cm.

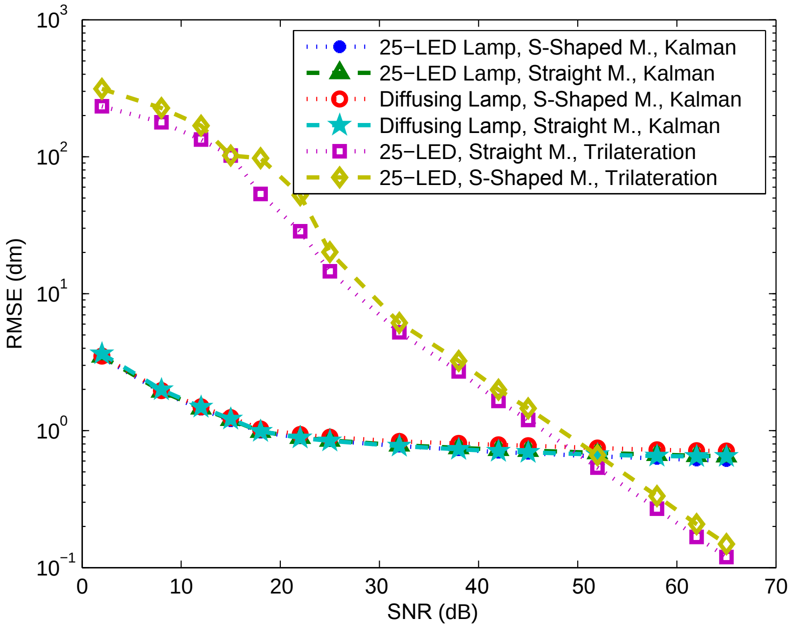

Figure 4.24: Comparison of trilateration and EKF when grid resolution is 1 dm.

The grid resolution is 1 dm in the simulations for Figure 4.24. The RMSE of the 25-LED lamp model and chandelier model is close to each other. This is a result of the quantization error. The grid size is ten times larger than the results in Figure 4.23. The accuracy of the positioning decreases. The trilateration approach gives better results after a certain SNR level.

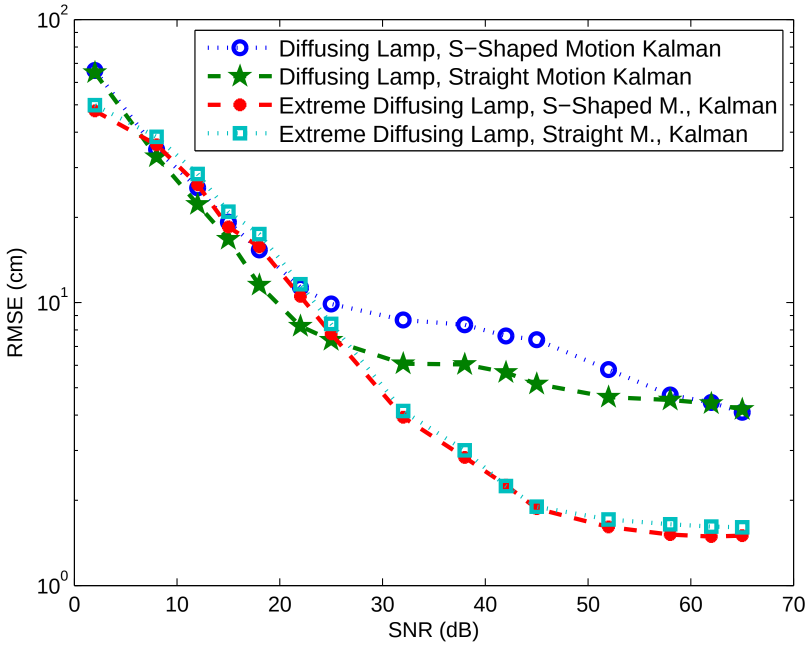

Figure 4.25: Comparison of diffuser and extreme diffuser.

In Figure 4.25, we compare an extreme diffuser scenario to regular diffuser scenario. Extreme diffuser means that there are tiny prisms that diffuse the light; an example of this can be the lamps that are used in the offices. The result shows that if we increase the diffusion, the tracking error will decrease.

Figures 4.26 and 4.27 show the comparison of RMSE for velocity for different SNR when the grid resolutions are 1 *cm* and 1 *dm*. From Figure 4.26, it can be seen that the lowest RMSE is achieved when the normal (deterministic) lamp is used. Figure 4.27 shows the RMSE of the velocity gets closer between the diffusing and the deterministic lamp when the grid resolution is increased.

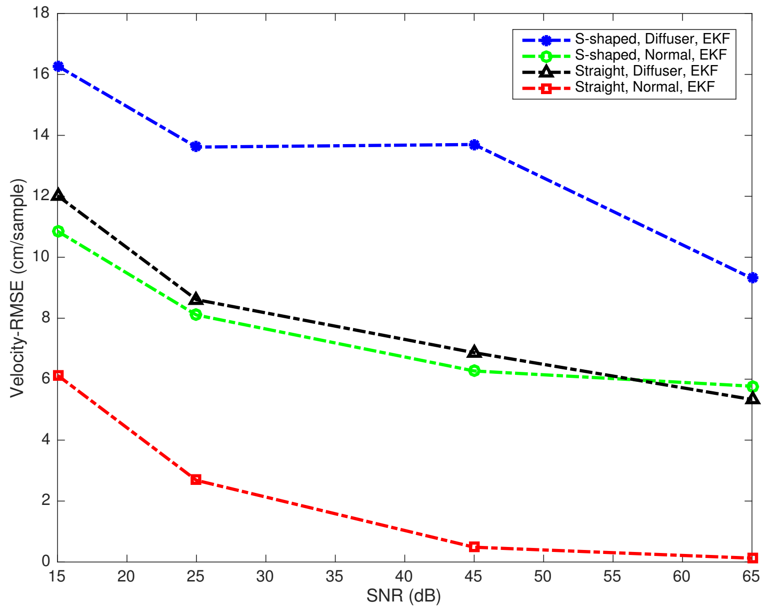

Figure 4.26: The RMSE of velocity when grid resolution is 1 *cm*.

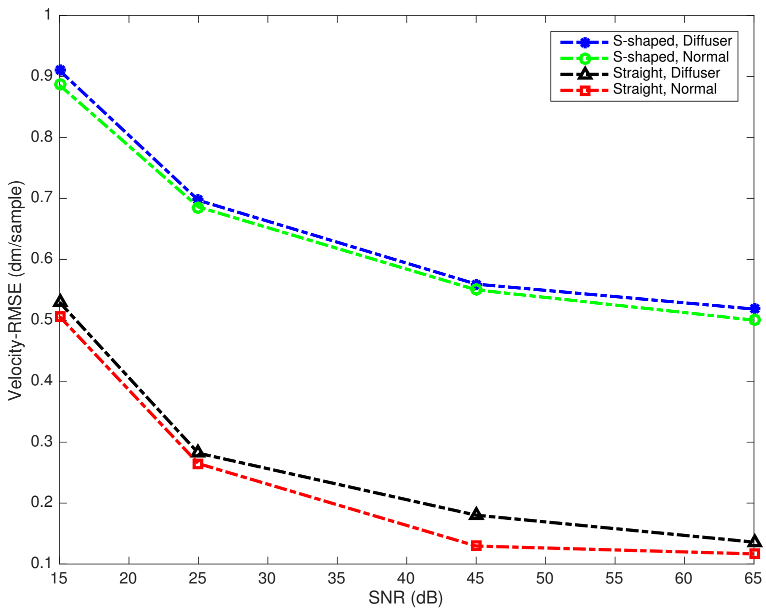

Figure 4.27: The RMSE of velocity when grid resolution is 1 *dm*.

Chapter 5

Conclusion and Future Work

5.1 Conclusion

High-speed indoor optical communication using LEDs is becoming more popular in the recent years. They have advantages like low power consumption, safety and they reduce the competition for bandwidth. Another contribution of VLC is in the field of indoor positioning. The summary of our research is as follows.

- We propose a new lamp model which imitates a chandelier. We modify previously proposed 25-LED lamp [21]. We compare the performance of two lamps for positioning purposes.
- Signal strength based methods store the RSS in the whole room as fingerprints, then matching is done between the RSS on the receiver and fingerprints. We use an EKF for processing RSS and fingerprints instead of matching.
- Previous studies generally covered the noise only caused by the receiver, in our work we not only take receiver noise but also system noise into account.

- In our simulations, we showed that the EKF approach performs better than the trilateration approach. The results show that even in random illumination maps due to the use of a diffuser, the EKF position errors are around 40 cm.
- We explained the accurate positioning is not possible with the trilateration approach when a diffusing lamp is used.

5.2 Future Work

The extension of our research is possible for future work. We do not have an accurate model for the noise in the system. A future investigation of the noise sources in the room environment is possible. We also can investigate the performance of other state estimation tools like unscented Kalman filter (UKF) and particle filter. An extension of this study may be with image processing; we will investigate the possible solution to match between the power distribution map and captured images with a camera placed at the transmitters. Another possible study is to investigate the effects of multiple receivers.

Bibliography

[1] R. E. Kalman, "A new approach to linear filtering and prediction problems," *Journal of Fluids Engineering*, vol. 82, no. 1, pp. 35–45, 1960.

[2] Z. Ghassemlooy, W. Popoola, and S. Rajbhandari, *Optical Wireless Communications:System and Channel Modeling with Matlab.* CRC Press, 2012.

[3] D. Dardari, P. Closas, and P. Djuric, "Indoor tracking: Theory, methods, and technologies," *Vehicular Technology, IEEE Transactions on*, vol. 64, no. 4, pp. 1263–1278, April 2015.

[4] H. Liu, H. Darabi, P. Banerjee, and J. Liu, "Survey of wireless indoor positioning techniques and systems," *Systems, Man, and Cybernetics, Part C: Applications and Reviews, IEEE Transactions on*, vol. 37, no. 6, pp. 1067–1080, Nov 2007.

[5] N. Patwari, J. Ash, S. Kyperountas, A. Hero, R. Moses, and N. Correal, "Locating the nodes: cooperative localization in wireless sensor networks," *Signal Processing Magazine, IEEE*, vol. 22, no. 4, pp. 54–69, July 2005.

[6] Y. B. Bai, S. Wu, H. Wu, and K. Zhang, "Overview of RFID-based indoor positioning technology," in *Proceedings of the Geospatial Science Research Symposium. Melbourne: RMIT University*, 2012.

[7] S. Chawathe, "Beacon placement for indoor localization using Bluetooth," in *Intelligent Transportation Systems, 2008. ITSC 2008. 11th International IEEE Conference on*, Oct 2008, pp. 980–985.

[8] T. Komine and M. Nakagawa, "Fundamental analysis for visible-light communication system using LED lights," *Consumer Electronics, IEEE Transactions on*, vol. 50, no. 1, pp. 100–107, Feb 2004.

[9] J. Armstrong, Y. Sekercioglu, and A. Neild, "Visible light positioning: a roadmap for international standardization," *Communications Magazine, IEEE*, vol. 51, no. 12, pp. 68–73, December 2013.

[10] M. Kavehrad and Z. W., "Light positioning systems (LPS)," in *Visible Light Communication*, S. Arnon, Ed. Cambridge University Press, 2015, pp. 70–85.

[11] W. Zhang, M. I. S. Chowdhury, and M. Kavehrad, "Asynchronous indoor positioning system based on visible light communications," *Optical Engineering*, vol. 53, no. 4, p. 045105, 2014. [Online]. Available: http://dx.doi.org/10.1117/1.OE.53.4.045105

[12] G. Prince and T. Little, "A two phase hybrid RSS/AOA algorithm for indoor device localization using visible light," in *Global Communications Conference (GLOBECOM), 2012 IEEE*, Dec 2012, pp. 3347–3352.

[13] L. Li, P. Hu, C. Peng, G. Shen, and F. Zhao, "Epsilon: A visible light based positioning system," in *11th USENIX Symposium on Networked Systems Design and Implementation (NSDI 14)*. Seattle, WA: USENIX Association, Apr. 2014, pp. 331–343. [Online]. Available: https://www.usenix.org/conference/nsdi14/technical-sessions/presentation/li

[14] S.-Y. Jung, S. Hann, S. Park, and C.-S. Park, "Optical wireless indoor positioning system using light emitting diode ceiling lights," *Microwave and Optical Technology Letters*, vol. 54, no. 7, pp. 1622–1626, 2012. [Online]. Available: http://dx.doi.org/10.1002/mop.26880

[15] Y. U. Lee and M. Kavehrad, "Two hybrid positioning system design techniques with lighting leds and ad-hoc wireless network," *Consumer Electronics, IEEE Transactions on*, vol. 58, no. 4, pp. 1176–1184, November 2012.

[16] S.-Y. Jung, S. Hann, and C.-S. Park, "TDOA-based optical wireless indoor localization using led ceiling lamps," *Consumer Electronics, IEEE Transactions on*, vol. 57, no. 4, pp. 1592–1597, November 2011.

[17] M. Rahaim, G. Prince, and T. Little, "State estimation and motion tracking for spatially diverse VLC networks," in *Globecom Workshops (GC Wkshps), 2012 IEEE*, Dec 2012, pp. 1249–1253.

[18] S.-H. Yang, H.-S. Kim, Y.-H. Son, and S.-K. Han, "Three-dimensional visible light indoor localization using AOA and RSS with multiple optical receivers," *J. Lightwave Technol.*, vol. 32, no. 14, pp. 2480–2485, Jul 2014. [Online]. Available: http://jlt.osa.org/abstract.cfm?URI=jlt-32-14-2480

[19] Y.-S. Kuo, P. Pannuto, K.-J. Hsiao, and P. Dutta, "Luxapose: Indoor positioning with mobile phones and visible light," in *Proceedings of the 20th Annual International Conference on Mobile Computing and Networking*, ser. MobiCom '14. New York, NY, USA: ACM, 2014, pp. 447–458. [Online]. Available: http://doi.acm.org/10.1145/2639108.2639109

[20] A. Sahin, Y. S. Eroglu, I. Güvenç, N. Pala, and M. Yuksel, "Hybrid 3d localization for visible light communication systems," *CoRR*, vol. abs/1508.05776, 2015. [Online]. Available: http://arxiv.org/abs/1508.05776

[21] J. Lian, "Multiuser miso indoor visible light communications," Master's thesis, University of Virginia, Charlottesville, 2014.

[22] J. Kahn and J. Barry, "Wireless infrared communications," *Proceedings of the IEEE*, vol. 85, no. 2, pp. 265–298, Feb 1997.

[23] K. Lee and H. Park, "Channel model and modulation schemes for visible light communications," in *Circuits and Systems (MWSCAS), 2011 IEEE 54th International Midwest Symposium on*, Aug 2011, pp. 1–4.

[24] M. Noshad and M. Brandt-Pearce, "Application of expurgated PPM to indoor visible light communications - part I: single-user systems," *CoRR*, vol. abs/1309.0750, 2013. [Online]. Available: http://arxiv.org/abs/1309.0750

[25] F. C. Comissions, "Location-based services: An overview of opportunities and other considerations," 2012. [Online]. Available: https://www.fcc.gov/document/location-based-services-report

[26] M. Bshara, U. Orguner, F. Gustafsson, and L. Van Biesen, "Fingerprinting localization in wireless networks based on received-signal-strength measurements: A case study on wimax networks," *Vehicular Technology, IEEE Transactions on*, vol. 59, no. 1, pp. 283–294, Jan 2010.

[27] F. Gustafsson and F. Gunnarsson, "Positioning using time-difference of arrival measurements," in *Acoustics, Speech, and Signal Processing, 2003. Pro-*

ceedings. (ICASSP '03). 2003 IEEE International Conference on, vol. 6, April 2003, pp. VI–553–6 vol.6.

[28] H. Liu, H. Darabi, P. Banerjee, and J. Liu, "Survey of wireless indoor positioning techniques and systems," *Systems, Man, and Cybernetics, Part C: Applications and Reviews, IEEE Transactions on*, vol. 37, no. 6, pp. 1067–1080, Nov 2007.

[29] K. Panta and J. Armstrong, "Indoor localisation using white LEDs," *Electronics Letters*, vol. 48, no. 4, pp. 228–230, February 2012.

[30] T. Tanaka and S. Haruyama, "New position detection method using image sensor and visible light LEDs," in *Proceedings of the 2009 Second International Conference on Machine Vision*, ser. ICMV '09. Washington, DC, USA: IEEE Computer Society, 2009, pp. 150–153. [Online]. Available: http://dx.doi.org/10.1109/ICMV.2009.44

[31] G. Welch and G. Bishop, "An introduction to the Kalman filter," Chapel Hill, NC, USA, Tech. Rep., 1995.

[32] T. K. Yaakov Bar-Shalom, X. Rong Li, *Estimation with Applications to Tracking and Navigation: Theory Algorithms and Software.* Wiley Press, 2001.

[33] M. Kohler, "Using the Kalman filter to track human interactive motion – modelling and initialization of the Kalman filter for translational motion," Tech. Rep., 1997.

[34] G. P. Agrawal, *Fiber Optic Communication Systems.* Wiley Series in Microwave and Optical Engineering, 2010.